Prepared for submission to JHEP

Bound-state beta decay of tritium: Path to first observation and novel approach to direct neutrino mass measurement

Evgeny Akhmedov,[a] **Thierry Lasserre,**[a] **Ferenc Glück**[b] **and Alejandro Saenz**[c]

[a] *Max-Planck-Institut für Kernphysik, Saupfercheckweg 1, 69117 Heidelberg*

[b] *Institute for Astroparticle Physics, Karlsruhe Institute of Technology, Hermann-von-Helmholtz-Platz 1, 76344 Eggenstein-Leopoldshafen, Germany*

[c] *AG Moderne Optik, Institut für Physik, Humboldt-Universität zu Berlin, Newtonstr. 15, 12489 Berlin, Germany*

E-mail: akhmedov@mpi-hd.mpg.de, thierry.lasserre@mpi-hd.mpg.de, ferenc.glueck@kit.edu, Alejandro.Saenz@physik.hu-berlin.de

Abstract: Bound-state β-decay of tritium, the process, in which the final-state electron is created in a bound atomic state of the produced ^{3}He atom instead of freely flying away, is predicted by the standard theory of weak interactions but has not been observed so far. We study the possibility of its experimental observation through the detection of photons from radiative decay of the excited atomic states of neutral ^{3}He populated by this process. We also propose a novel approach to direct neutrino mass measurement and sterile neutrino search based on accurate determination of the speed of the produced ^{3}He atoms through Doppler broadening of the emitted photon lines.

arXiv:2607.24928v1 [hep-ph] 27 Jul 2026

Contents

1 Introduction **1**

2 Tritium BSBD observation **3**
- 2.1 ^{3}He atomic states and radiative transitions relevant for BSBD 3
- 2.2 Radiative and collisional de-excitation of ^{3}He. Event rates 6

3 Backgrounds **7**
- 3.1 CSBD and irreducible backgrounds 7
- 3.2 Accidental backgrounds and their rejection 9

4 Direct neutrino mass measurements through ^{3}He speed determination **9**
- 4.1 Neutrino mass and ^{3}He velocities 9
- 4.2 Neutrino mass measurement through the Doppler effect 10
- 4.3 Statistical requirements in the limit of vanishing natural linewidths 12
- 4.4 Effects of finite natural widths of the excited states of ^{3}He 14
- 4.5 Statistical requirements with finite linewidths 15
- 4.6 Effects of thermal motion of parent tritium atoms 17

5 Summary and discussion **21**

A 2-body decay and the speed of ^{3}He **23**

B BSBD with a mixed atomic/molecular tritium source and background from CSBD **23**

C Statistical requirements for neutrino mass measurements **26**

1 Introduction

Bound-state β-decay (BSBD) is the nuclear β^--decay process in which the electron is created bound to a vacant atomic orbital of the final-state atom rather than in the continuum. It was first predicted in the late 1940s [1, 2] and thereafter has been extensively studied theoretically (see e.g. [3–14]). BSBD was first experimentally observed in 1992 in fully ionized ^{163}Dy [15], and has subsequently been detected in three additional fully ionized atomic species – ^{187}Re, ^{207}Tl and ^{205}Tl [16–18]. The standard weak interaction theory predicts that tritium should experience BSBD as well, with relatively large branching ratio with respect to the usual, continuum-state β-decay (CSBD): $\Gamma_{\rm BSBD}/\Gamma_{\rm CSBD} = \mathcal{O}(1\%)$. However, this process has not been observed so far.

BSBD of atomic tritium,

$$\mathrm{T} \rightarrow {}^3\mathrm{He} + \bar{\nu}_e \,, \tag{1.1}$$

creates a neutral ^{3}He atom and an electron antineutrino in the final state. As the $\bar{\nu}_e$ is practically unobservable, the process can only be observed through the detection of ^{3}He. In this paper we suggest a way of doing this. Calculations show that a significant fraction of ^{3}He atoms are produced in several low-lying excited states. Their subsequent radiative decays produce characteristic atomic photons that can be readily detected, providing a clear signature of tritium BSBD.

More importantly, this opens up a novel possibility of direct neutrino mass measurement. Two-body nature of the final state of process (1.1) implies that, for a fixed neutrino mass, the produced ^{3}He atoms and $\bar{\nu}_e$ are monoenergetic. The velocities of ^{3}He exhibit a weak dependence on neutrino mass; therefore, accurate measurements of these velocities would determine neutrino masses.

How can the velocities of the produced ^{3}He be determined? Time-of-flight techniques cannot be used in this case, as the instant of time when the decay of the parent tritium occurred is unknown, and there is no electron emission that could be used as a time tag. However, the velocities of ^{3}He atoms produced in excited atomic states can be determined through Doppler broadening of the lines of the emitted photons. Thus, the same radiative decay processes that can be used for the observation of BSBD of tritium can also be employed for probing neutrino masses. The requirements for these two types of experiments are, however, different. While for observation of tritium BSBD it is sufficient to detect the characteristic ^{3}He de-excitation photons (provided that backgrounds are under control), in order to probe neutrino masses one has to measure very accurately the lineshapes of the emitted photons. This is much more demanding. The current state-of-the-art in quantum optics allows atomic frequency measurements with accuracies reaching $\Delta\omega/\omega_0 \sim 10^{-18}$ [19, 20]. The accuracies of lineshape measurements are more modest, currently in the $10^{-4} - 10^{-11}$ range [21–23], but progress in this field is very fast. In addition to very accurate lineshape measurements, cryogenic temperatures will be necessary in order to suppress thermal motion of the parent tritium atoms.

Since electron antineutrinos produced in BSBD are linear superpositions of different neutrino mass eigenstates, the lineshapes of the individual photon lines should exhibit characteristic kinks, similarly to the kinks in the electron spectra sought in CSBD experiments [24–26]. There are, however, important differences. While direct neutrino mass measurement experiments based on nuclear β-decay usually measure electron energies near the endpoint of the spectrum, our proposal relies on photon frequency measurements. In this respect it is similar to approaches based on cyclotron radiation emission spectroscopy (CRES), such as Project 8 [27] or QTNM [28]. What sets our approach apart from all CSBD-based neutrino mass measurements is the scaling of the relative number of events in the neutrino-mass-sensitive region: this fraction scales as $(m_\nu/Q)^2$, whereas in CSBD-based experiments it scales as $(m_\nu/Q)^3$ (where Q is the Q-value of the process). Thus, the number of "useful" events is increased by a very large factor of Q/m_ν, which is a direct consequence of the two-body decay kinematics in BSBD, as opposed to the three-body kinematics of the

ordinary β-decay.

Direct neutrino mass measurement experiments based on orbital electron capture (EC) [29–31] also involve two-body final states. However, EC produces highly excited daughter atoms that de-excite via X-ray cascades and Auger electrons, requiring calorimetric measurements for precise determination of the released energy. In contrast, BSBD leaves the final-state atoms in the ground state or in low-lying excited states; the latter de-excite by emitting optical or extreme ultraviolet (XUV) photons, which are much easier to detect.

In this paper we focus primarily on the conceptual issues and general aspects of the proposed observation of BSBD of tritium via detection of photons coming from de-excitation of the final-state ^{3}He atoms, as well as of the novel approach to direct neutrino mass measurement that it offers. We do not discuss specific experimental setups or the associated systematic uncertainties, as these lie outside the scope of the present work and will be addressed in future studies.

The units $\hbar = c = 1$ are used throughout the paper.

2 Tritium BSBD observation

2.1 ^{3}He atomic states and radiative transitions relevant for BSBD

The rate of BSBD of atomic tritium has been evaluated by a number of authors. To our knowledge, the most accurate calculations were carried out in Ref. [7], where the BSBD branching ratio was found to be $\Gamma_{\rm BSBD}/\Gamma_{\rm CSBD} = 0.55\%$. The authors also calculated separately the fractions of BSBD transitions to the ground state and to a number of excited states of the final-state neutral ^{3}He atoms. In Table 1 we present these fractions for the ground state as well as for $1s2s$ and $1s3s$ excited states of ^{3}He (combined singlet and triplet), which together constitute over 95% of all BSBD transitions. The branching fractions of the excited states should be distributed between singlet and triplet ^{3}He statistically, with the ratio 1:3.

Final atomic state of ^{3}He	**Branching fraction**
$1s^2$ ground state (singlet)	57%
$1s2s$ states (singlet+triplet)	32.5%
$1s3s$ states (singlet+triplet)	5.6%

Table 1: Fractions of tritium BSBD transitions to the ground state and a few excited states of ^{3}He [7].

The level schemes of singlet and triplet ^{3}He atoms as well as radiative decays of interest are shown in Figure 1. We summarize the properties of the relevant states and transitions in Table 2. The options for the observation of BSBD of tritium include:

I. *Detection of photons from radiative decays of singlet or triplet* $1s2s$ *states.*

(a) The singlet $1s2s$ state decays to the $1s^2$ ground state by emitting a pair of E1 photons (single photon emission is highly suppressed). Coincidence detection of photon pairs whose energies satisfy $\omega_1 + \omega_2 = E_{\rm exc.} = 20.62$ eV could serve as a signature of BSBD.

There are, however, certain limitations related to this channel. At least one of the two photons in the emitted pair is in the XUV range, typically both. Detecting such photons is more difficult than detecting e.g. optical photons; in addition, energy resolution of XUV photon detectors is at best marginal. Up to now, radiative decays of the singlet $1s2s$ states of neutral helium atoms (either ^{3}He or ^{4}He) have not been directly observed. Their lifetime, $\tau \simeq 20$ ms, has only been measured indirectly through time-of-flight techniques. In addition to the already mentioned poor energy resolution of photodetectors in the XUV region, the observation is complicated by the fact that coincident detection requires strong sources (sufficient amount of excited helium is needed). This, however, does not seem

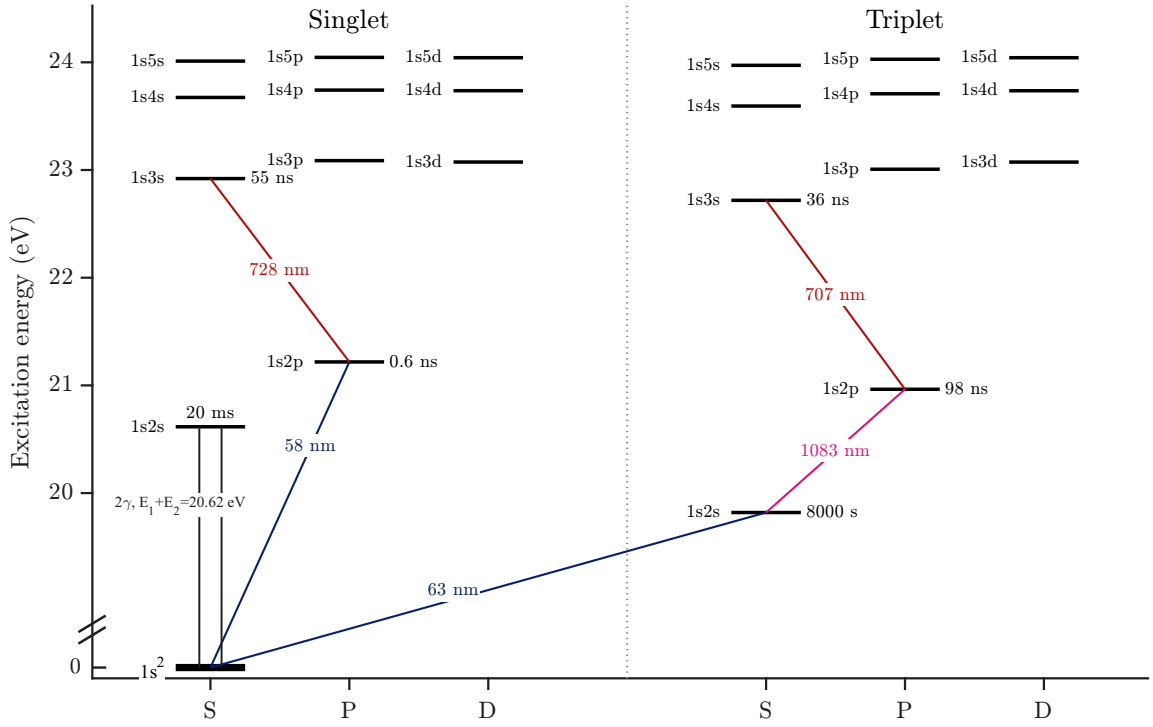

Figure 1: Partial atomic level schemes for singlet (left) and triplet (right) ^{3}He atoms. Atomic transitions of interest are shown by colored lines. The data are taken from [32].

to constitute a problem in tritium β-decay experiments such as KATRIN [25]: BSBD of tritium is expected to produce very large amounts of singlet ^{3}He atoms in the metastable $1s2s$ state. Moreover, lack of energy resolution of XUV photodetectors may to some extent be mitigated by coincidence detection provided that a good time resolution can be achieved. Thus, if BSBD is identified via this channel, this will not only be an observation of tritium BSBD, but also the first direct observation of 2-photon decay of the singlet $1s2s$ metastable state or helium. *(b)* The triplet $1s2s$ excited states of ^{3}He decay to the $1s^2$ ground state by emitting a single M1 photon with energy $\omega = 19.82$ eV (wavelength $\lambda = 62.56$ nm, in the XUV range). The observation of this transition faces the same difficulties with XUV photon detection as the decay of the singlet $1s2s$ state. In addition, the triplet $1s2s$ state is extremely long-lived ($\tau = 7870$ s), which makes it particularly vulnerable to collisional de-excitation and thus very difficult to observe via radiative decay.

II. *Detection of photons from radiative decays of singlet or triplet* $1s3s$ *states to the correspond-*

State	$\mathbf{E}_{\text{exc.}}$ (eV)	$\boldsymbol{\tau}$	Decay mode	$\mathbf{E}_{\text{decay}}$ (eV)	Wavelength
singlet $1s2s$	20.62	20 ms	$1s2s \to 1s^2$(g.s.), 2γ, E1, $\omega_1 + \omega_2 = E_{\text{exc.}}$	20.62	continuum
triplet $1s2s$	19.82	7870 s	$1s2s \to 1s^2$(g.s.), M1	19.82	62.56 nm (XUV)
singlet $1s3s$	22.93	54.64 ns	$1s3s \to 1s2p$(singl.), E1	1.703	728.1 nm (Red)
triplet $1s3s$	22.72	35.92 ns	$1s3s \to 1s2p$(tripl.), E1	1.755	706.5 nm (Red)
singlet $1s2p$	21.23	0.56 ns	$1s2p \to 1s^2$(g.s.), E1	21.23	58.4 nm (XUV)
triplet $1s2p$	20.96	98 ns	$1s2p \to 1s2s$(tripl.), E1	1.145	1083 nm (NIR)

Table 2: Properties of the relevant ^{3}He excited states and their radiative de-excitation transitions [32]. The table lists the excitation energy $E_{\text{exc.}}$, lifetime τ, decay mode, transition type, radiative decay energy E_{decay}, and photon wavelength for each state.

ing $1s2p$ *states.*

These transitions are very similar in singlet and triplet ^{3}He. The singlet $1s3s$ state (lifetime $\tau = 54.64$ ns) decays to the singlet $1s2p$ state by emitting an E1 photon with energy $\omega = 1.703$ eV (wavelength $\lambda = 728.1$ nm). The triplet $1s3s$ state (lifetime $\tau = 35.92$ ns) decays to the triplet $1s2p$ state by emitting an E1 photon with energy $\omega = 1.755$ eV (wavelength $\lambda = 706.5$ nm).[1] Both transitions correspond to the well-known red lines of neutral helium, which are routinely observed in atomic spectroscopy and are often used for plasma diagnostics and in astrophysical studies.

III. *Detection of photons from radiative decays of singlet or triplet* $1s2p$ *states populated by the preceding decays of the corresponding* $1s3s$ *states.*

(a) The singlet $1s2p$ state decays almost exclusively (with branching ratio 99.9%) to the ground state of ^{3}He by emitting an E1 photon with energy $\omega = 21.23$ eV (wavelength $\lambda = 58.4$ nm, in the XUV range). The lifetime of this state is very short, $\tau = 0.56$ ns.

(b) The triplet $1s2p$ state decays to the $1s2s$ state of triplet helium by emitting an E1 photon with energy $\omega = 1.145$ eV (wavelength $\lambda = 1083$ nm). The lifetime of the initial state is $\tau = 98$ ns. This transition corresponds to the well-known near-infrared (NIR) line in the helium spectrum which is widely used for precision tests of quantum electrodynamics, laser cooling and trapping of helium, and in astrophysical studies.

IV. *Detection of sequences of radiative transitions in prompt or delayed coincidence.*

To reject possible accidental backgrounds, coincidence detection of photons emitted in the following sequences of transitions may also be helpful:

1. Red and NIR photons from the transitions in triplet ^{3}He:

$$1s3s \xrightarrow{706.5\,\text{nm}} 1s2p \xrightarrow{1083\,\text{nm}} 1s2s \tag{2.1}$$

[1] In triplet helium, $1s2p$ actually denotes a triplet of fine-structure states with angular momenta $J = 0, 1, 2$ (denoted $1s2p\,^3P_{0,1,2}$), separated by very small energy intervals, $\sim 10^{-4}$ eV. The $1s3s \to 1s2p$ transitions thus produce a triplet of nearly degenerate red lines. However, these can currently only be resolved by high-resolution laser spectroscopy, so their splitting is irrelevant for BSBD observation. The same holds for near-infrared $1s2p \to 1s2s$ transitions in triplet helium discussed in point III(b) below. Fine-structure splitting of triplet helium lines should, however, be taken into account in probing neutrino masses via Doppler emission spectroscopy as discussed in section 4. It will will not hinder the neutrino mass measurements.

in delayed coincidence (lifetime of the $1s2p$ state $\sim 100\,\mathrm{ns}$).

2. Red and XUV photons from the transitions in singlet ^{3}He:

$$1s3s \xrightarrow{728.1\,\mathrm{nm}} 1s2p \xrightarrow{58.4\,\mathrm{nm}} 1s^2 \tag{2.2}$$

in prompt coincidence (lifetime of the $1s2p$ state $\sim 0.6\,\mathrm{ns}$).

Summarizing, the most promising approaches for observing BSBD of tritium appear to be

- Detection of red-line photons from the $1s3s \to 1s2p$ transitions in either triplet or singlet ^{3}He (or both)
- Detection of NIR photons from the $1s2p \to 1s2s$ transitions in triplet ^{3}He
- Delayed coincidence detection of red and NIR photons in triplet ^{3}He [eq. (2.1)]
- Prompt coincidence detection of red and XUV photons in singlet ^{3}He [eq. (2.2)]

These transitions are shown in Fig. 1 by colored lines.

2.2 Radiative and collisional de-excitation of ^{3}He. Event rates

We now estimate the expected numbers of events for the proposed observation of BSBD of tritium. We assume an atomic tritium source with activity 10^8 Bq, corresponding to $N_0 = 5.6 \times 10^{16}$ tritium atoms (10^{-3} of the amount used in the KATRIN experiment).[2]

From the tritium CSBD rate $\Gamma_1 = (17.75\,\mathrm{yr})^{-1} = 1.786 \times 10^{-9}\,\mathrm{s}^{-1}$ and the BSBD branching ratio of 0.55%, one finds the total BSBD rate $\Gamma_{\mathrm{BSBD}} = 9.89 \times 10^{-12}\ \mathrm{s}^{-1}$.

We denote by Γ_2 the BSBD production rate of ^{3}He atoms in a specific excited atomic state under study. For definiteness, we focus below on the production of ^{3}He in the triplet $1s3s$ excited state. From Table 1 we find

$$\Gamma_2 = 4.15 \times 10^{-13}\ \mathrm{s}^{-1}. \tag{2.3}$$

The production rates for the other excited states of ^{3}He atoms discussed above can also be readily obtained from Table 1.

Since the radiative decays of all excited ^{3}He states (including the metastable ones) are much faster than BSBD of tritium, the emission rate of ^{3}He de-excitation photons is dominated by BSBD. From eq. (2.3) we then obtain the photon production rate

$$\frac{dN_{\mathrm{ph}}}{dt} = N_0\Gamma_2 \simeq 23000\ \mathrm{s}^{-1}. \tag{2.4}$$

Thus, the number of events accumulated over 24 hours is $\simeq 2 \times 10^9$. The number of actually observed events will of course be smaller, since the incomplete coverage of the inner walls of the experimental cavity by photodetectors and the detection efficiency must be taken into account. Nevertheless, the expected event statistics remains very high.

In estimating the event numbers, we assumed that all excited ^{3}He atoms de-excite radiatively, i.e., we ignored possible collisional de-excitation. Let us now estimate its possible effects. Non-radiative relaxation of the excited states of ^{3}He atoms can occur through their collisions with either the inner walls of the experimental cavity or with other particles present in it, primarily undecayed tritium atoms. The velocity of the produced ^{3}He atoms is $v_0 \simeq 2$ km/s (see section 4.1). Assuming

[2] The cases of molecular and mixed atomic/molecular tritium sources are discussed in section 3.1 and Appendix B.

an experimental cell of linear size $L \sim 10$ cm, the average time for an excited ^{3}He atom to hit an inner wall and de-excite is

$$t_{c1} \simeq \frac{L}{v_0} \simeq 50\,\mu\text{s}\,. \tag{2.5}$$

Next, we estimate the characteristic time of ^{3}He de-excitation via collisions with tritium atoms. The tritium number density in a volume of $(10\,\text{cm})^3$ is

$$n_T = \frac{5.6 \times 10^{16}}{10^3\ \text{cm}^3} = 5.6 \times 10^{13}\text{cm}^{-3}. \tag{2.6}$$

Assuming a collisional de-excitation cross section $\sigma_c \simeq 10^{10}\,b = 10^{-14}\,\text{cm}^2$ (a conservative estimate), one finds

$$t_{c2} = (n_T \sigma_c v_0)^{-1} \simeq 10\ \mu\text{s}.$$

Comparing these de-excitation times with the radiative lifetimes of the excited ^{3}He states given in Table 2, one sees that, under the discussed conditions, the collisional de-excitation processes are much slower than radiative decay – and therefore can be safely neglected – for all excited helium states except the metastable $1s2s$ ones. For the singlet metastable state, BSBD observation might still be possible if detectors of significantly larger sizes are used; however, for the extremely long-lived triplet $1s2s$ state, collisional relaxation will likely dominate under any realistic experimental conditions.

3 Backgrounds

There are two types of possible backgrounds to BSBD of tritium that can hinder its unambiguous experimental observation:

- Backgrounds from processes different from BSBD but leading to the same excited states of neutral ^{3}He atoms as those we are interested in. These are irreducible backgrounds that can precisely mimic BSBD.

- Accidental backgrounds from other processes that could lead to similar signals (e.g. photons from bremsstrahlung in CSBD) in the case of insufficient detector energy or time resolution.

3.1 CSBD and irreducible backgrounds

(i) Production of neutral ^{3}He *in CSBD of* T_2.

Consider now the case of a molecular tritium source and the associated backgrounds to BSBD. One possible background is related to CSBD of molecular tritium,

$$T_2 \;\to\; {}^3\text{HeT}^+ + e^- + \bar{\nu}_e\,. \tag{3.1}$$

It produces molecular ions $^3\text{HeT}^+$, about half of which dissociate [33–36]. The main dissociation channels are (ref. [35], table V):

$${}^3\text{HeT}^+ \to \text{T}^+ + {}^3\text{He} \qquad (\sim 66\%)\,, \tag{3.2}$$

$${}^3\text{HeT}^+ \to \text{T} + {}^3\text{He}^+ \qquad (\sim 18\%)\,, \tag{3.3}$$

where the dissociation fractions are shown in the parentheses.[3] Other channels, such as e.g. double ionization of the produced ^{3}He, are not relevant to our discussion.

[3] The quoted dissociation fractions were obtained in the sudden approximation.

Channel (3.2) may populate, among others, the $1s2s$ or $1s3s$ excited states of neutral ^{3}He, if the molecular ions $^3HeT^+$ are produced in sufficiently high excited electronic states. This would create an irreducible background for the tritium BSBD observation method proposed here. Unfortunately, a reliable evaluation of the fraction of CSBD transitions in T_2 leading to such excited states is quite involved and is not currently available. Given that the tritium CSBD rate Γ_1 is three to four orders of magnitude larger than the partial BSBD rates Γ_2 of interest, even a modest fraction of $1s2s$ or $1s3s$ excited neutral ^{3}He atoms produced via channel (3.2) could make the observation of tritium BSBD using the approach suggested here essentially impossible in molecular tritium. In that case, one would need to search for tritium BSBD using atomic tritium sources.

Interestingly, the fraction of the "unwanted" CSBD processes leading to the excited ^{3}He state under study could, in principle, be probed experimentally with mixed atomic/molecular tritium sources, provided that the atomic-to-molecular ratio can be varied.[4] We concentrate here on the $1s3s$ states of singlet and triplet helium, for which collisional de-excitation can be neglected and the numbers of the emitted photons essentially coincide with the numbers of atoms produced in the corresponding excited states, as discussed in section 2.2. Assume that the initial total number of tritium atoms in the mixture is N_0, and that the atomic fraction is k. The mixture then contains $N_a = N_0 k$ tritium atoms and $N_m = \frac{1}{2}N_0(1-k)$ molecules. We denote by r the fraction of the CSBD transitions in molecular tritium that lead to the excited $1s3s$ states of neutral helium. The rate of these "unwanted" transitions is then $\Gamma_1 r$, and the number of events accumulated over a time interval t is

$$2N_m\Gamma_1 r t = N_0\Gamma_1 r(1-k)t\,. \tag{3.4}$$

We also need both the atomic and molecular rates of BSBD transitions to the excited atomic state under study. As discussed in section 2.1, the atomic rates Γ_2 are accurately known from the calculations; unfortunately, no calculations of BSBD rates in molecular tritium are available. We therefore parameterize the molecular BSBD rate (per constituent atom) for the transition with excitation of the relevant ^{3}He state as $(1-\delta)\Gamma_2$. The molecular BSBD rates are not expected to be drastically different from the corresponding atomic rates, i.e. one expects $1-\delta = \mathcal{O}(1)$. The total number of the atomic and molecular BSBD events accumulated over the time interval t is $N_0 t[\Gamma_2 k + (1-\delta)\Gamma_2(1-k)]$. Combining this with the CSBD contribution (3.4) and taking into account that the number of de-excitation photons coincides with that of the excited helium states, we find

$$N_{\rm ph} = N_0 t\Big[\Big(r - \frac{\Gamma_2}{\Gamma_1}\delta\Big)\Gamma_1(1-k) + \Gamma_2\Big]\,. \tag{3.5}$$

Because $\Gamma_2/\Gamma_1 \sim 10^{-4}$ and $\delta = \mathcal{O}(1)$ while r may be as large as a few percent [35], one can to a first approximation neglect the term $(\Gamma_2/\Gamma_1)\delta$ in eq. (3.5), which yields

$$N_{\rm ph} \simeq N_0 t[\Gamma_1 r(1-k) + \Gamma_2]\,. \tag{3.6}$$

Thus, by varying the atomic fraction k and studying the dependence of the number of emitted photons on $1-k$, one could in principle determine the value of r, which governs the irreducible background from CSBD of tritium. If the $(1-k)$-independent term in (3.6) can be reliably shown to be nonzero, this would constitute an unambiguous observation of tritium BSBD and the first experimental measurement of its partial rate Γ_2. See Appendix B for details.

It should be stressed that the above discussion of BSBD and CSBD for mixed molecular/atomic tritium sources is necessarily simplified and schematic. It does not take into account important experiment-specific effects, such as adsorption of molecular tritium on the inner walls of the exper-

[4] We are grateful to Sergey Vasiliev for this observation.

imental cavity or possible time dependence of the atomic fraction k. These features depend on the particular experimental setup and cannot be assessed in an experiment-independent way.

(ii) $^3\mathrm{He}^+ - e^-$ *recombination.*

According to ref. [35], about 10% of all CSBD transitions in molecular tritium produce singly charged helium ions $^3\mathrm{He}^+$ through the dissociation channel (3.3) of $^3\mathrm{HeT}^+$ molecular ions.[5] In the case of CSBD of atomic tritium, $^3\mathrm{He}^+$ ions are produced in 100% of the decays. Radiative recombination of these ions with free electrons present inside the experimental cavity produces neutral helium atoms. This process may populate, among others, the excited atomic states of ^{3}He of interest here, and therefore can be another source of irreducible background to BSBD of tritium. The total cross section of radiative recombination is, however, rather small: $\sigma_{rr} = 7.6 \times 10^{-18}\,\mathrm{cm}^2$ in the limit of vanishing electron velocity v_e, and it decreases rapidly with increasing v_e (see, e.g., [37]). The velocity distribution of electrons is experiment-dependent, and therefore the recombination rate cannot be assessed in a general way. If the background from $^3\mathrm{He}^+ - e^-$ recombination in a particular experiment is found to be of concern, electrons and $^3\mathrm{He}^+$ ions can be efficiently removed by applying suitably configured transient electric and magnetic fields.

3.2 Accidental backgrounds and their rejection

One possible source of accidental backgrounds in tritium BSBD experiments is inner bremsstrahlung accompanying CSBD of tritium. This process produces photons with energies ranging from zero up to 18.6 keV, a small fraction of which have energies overlapping with those of the atomic transitions in helium of interest here.

As an example, consider the red-line photons emitted in the radiative decays of the $1s3s$ states of singlet or triplet helium, discussed in section 2.1 (with energies 1.703 eV and 1.755 eV, respectively). Numerical calculations based on the standard theory of inner bremsstrahlung [38] show that the fractions of tritium CSBD events producing photons in the energy interval [1.5 eV, 2 eV] is approximately 10^{-5}, which is about a factor of 20 smaller than the BSBD branching ratios for the excitation of the $1s3s$ states of ^{3}He. This background can be further suppressed by using optical filters to reduce the spectral window for photon detection. To a good accuracy, it can be neglected; since it is small and accurately known, it can also be simply subtracted.

In general, accidental backgrounds of various origins can be suppressed by using narrow-bandpass optical filters. Accidentals can also be efficiently rejected by detecting prompt or delayed coincidences between the photons from the cascade decays $1s3s \to 1s2p \to 1s^2$ in singlet helium or $1s3s \to 1s2p \to 1s2s$ in triplet helium, as discussed in section 2.1.

4 Direct neutrino mass measurements through ^{3}He speed determination

We now consider the possibility of determining neutrino mass by measuring the velocities of ^{3}He atoms produced in tritium BSBD. In what follows, we restrict ourselves to BSBD of atomic tritium.

4.1 Neutrino mass and ^{3}He velocities

For a given neutrino mass, the velocity of a neutral ^{3}He produced in tritium BSBD has a fixed value in the tritium's rest frame. It is defined by the kinematics of two-body decay, and in the limit of vanishing neutrino mass is given by

$$v_0 = \frac{Q}{M} \simeq 1.986\,\mathrm{km/s}\,. \tag{4.1}$$

[5] This follows from eq. (3.3), taking into account that only about 50% of the produced molecular ions $^3\mathrm{HeT}^+$ dissociate.

Here $M \equiv (M_i^2 + M_f^2)/(M_i + M_f)$, where M_i and M_f are the atomic masses of tritium and ^{3}He. The Q-value of the process is the difference of these masses: $Q = M_i - M_f \simeq 18.6\,\mathrm{keV}$. For transitions to an excited atomic state of ^{3}He with the excitation energy E_{exc}, the quantity M_f must be replaced by $M(^3\mathrm{He}) + E_{\mathrm{exc}}$, and the Q-value of the process must be modified accordingly. For tritium BSBD with the production of neutrino mass eigenstate ν_k of mass m_k, the velocity of the final-state helium atom is

$$v_k \simeq \frac{\sqrt{Q^2 - m_k^2}}{M} \approx v_0\Big(1 - \frac{m_k^2}{2Q^2}\Big)\,. \tag{4.2}$$

The first approximate equality here holds to an accuracy of about 10^{-11}; the exact relation is given in Appendix A. The velocity change of the produced helium atom due to nonzero neutrino mass is

$$\Delta v \equiv v_0 - v_k \simeq \frac{m_k^2}{2MQ} \simeq 2.87 \times 10^{-4}\,(m_k/\mathrm{eV})^2\,\mathrm{cm/s}\,. \tag{4.3}$$

Thus, the velocity of the ^{3}He atom is reduced relative to v_0 by about 3 m/s for a keV-scale (sterile) neutrino, but only by $\sim$7 nm/s for $m_k \simeq 50\,\mathrm{meV}$, which corresponds to the mass of the heaviest active neutrino.

4.2 Neutrino mass measurement through the Doppler effect

The idea of using the Doppler effect to observe tritium BSBD and probe neutrino masses was first proposed in ref. [6]. The authors suggested using tunable lasers to excite the metastable singlet helium (produced in tritium BSBD with a sizable branching ratio) from the $1s2s$ state to the $1s3p$ state and to detect the subsequent de-excitation photons. The laser can be tuned to this transition approximately; if the detuning is sufficiently small, it can be compensated by the Doppler shift arising from the nonzero velocity of the excited helium atoms. By scanning the detuning, one can determine this velocity. The method is thus based on laser-induced fluorescence and Doppler absorption spectroscopy.

The advantage of this approach is that the resonant spectroscopy allows photon frequency measurements with extremely high resolution. The method, however, has some limitations: small irradiation areas and additional line broadening sources, such as power broadening and transit time broadening.

In contrast, our approach relies on Doppler emission spectroscopy: we propose to accurately measure the profiles of the emission lines of the excited helium atoms corresponding to the transitions discussed in section 2.1. The relevant excited states of ^{3}He are populated by tritium BSBD itself, and no laser-induced optical pumping is required.

We first consider the case when the velocities of the parent tritium atoms are negligibly small. The effects of thermal motion of tritium will be discussed in section 4.6.

The profile of a photon line emitted by an isolated excited atom at rest has the Lorentzian form:

$$L(\omega) = \frac{\Gamma/2\pi}{(\omega - \omega_0)^2 + \Gamma^2/4}\,. \tag{4.4}$$

Here ω_0 is the central frequency of the line and Γ is the sum of the natural linewidths of the initial and final atomic states.

If the parent atom moves with speed v, the lineshape is modified by the Doppler effect. To linear order in v/c, one finds

$$L_{v,\cos\theta}(\omega) = \frac{\Gamma/2\pi}{(\omega - \omega_0 - \omega_0 \frac{v}{c}\cos\theta)^2 + \Gamma^2/4}\,. \tag{4.5}$$

The Doppler shift $\omega_0 \frac{v}{c} \cos\theta$ depends on the angle θ between the velocity of the excited helium atom and the direction of photon emission. Since BSBD of tritium produces helium atoms with isotropically distributed velocities, one must average the lineshape (4.5) over $\cos\theta$, which yields

$$F(\Delta; a, \Gamma) \equiv \frac{1}{2} \int_{-1}^{1} d\cos\theta L_{v,\cos\theta}(\omega) = \frac{1}{2\pi a} \left\{ \arctan\left[\frac{2(\Delta + a)}{\Gamma}\right] - \arctan\left[\frac{2(\Delta - a)}{\Gamma}\right] \right\}. \quad (4.6)$$

Here

$$\Delta \equiv \omega - \omega_0 \,, \qquad a \equiv (v/c)\omega_0 \,. \quad (4.7)$$

In the limit $v \to 0$ (*i.e.* $a \to 0$) the Lorentzian profile (4.4) is recovered. For small natural linewidths ($\Gamma \ll |\Delta|, a$), one obtains

$$F(\Delta; a, \Gamma \ll |\Delta|) \simeq \frac{1}{2a} \begin{cases} 1, & |\Delta| \le a \\ 0, & |\Delta| > a \end{cases} , \quad (4.8)$$

that is, the line has a rectangular shape. Taking into account small natural widths of the initial and final atomic states would smooth the corners of the rectangle.

Thus, the width of the spectral line is in this case fully determined by the Doppler broadening effect, despite the fact that the speed v of the excited atom is fixed; the spread of the Doppler shifts is entirely due to the spread in the values of the angle θ rather than due to the thermal motion of the excited ^{3}He atoms. The line profile is therefore different from the usual Voigt profile, which is a convolution of the Lorentzian and Gaussian distributions.

The parameter a in eq. (4.7) is the maximum Doppler shift of the photon frequency, corresponding to $\cos\theta = \pm 1$. It defines the positions of the edges of the rectangular line profile of the emitted photons. For a nonzero neutrino mass, this parameter decreases by $(\Delta v/c)\omega_0$ compared to the massless neutrino case. From eq. (4.3) it then follows that the relative change in the position of the spectral line's edge due to nonzero neutrino mass is

$$\frac{\Delta\omega_{\max}}{\omega_0} = \frac{\Delta v}{c} \simeq 9.6 \times 10^{-15} (m_\nu/\mathrm{eV})^2 \,. \quad (4.9)$$

Because electron antineutrinos produced in BSBD are linear superpositions of neutrino mass eigenstates ν_k, the lineshape of the emitted photon line is the weighted sum of the rectangles corresponding to different ν_k, with weights given by the squared matrix elements of the leptonic mixing matrix, $|U_{ek}|^2$. The resulting photon line profile will therefore exhibit kinks (smoothed steps) at the frequencies corresponding to the onsets of the contributions of neutrinos of different masses. This is illustrated in Fig. 2, which shows the photon line profile for the case of one massless and one massive neutrino species in the limit of vanishingly small natural linewidths. This is a good first approximation for the case of a fourth, predominantly sterile, neutrino state, whose mass is significantly larger than those of the ordinary active neutrinos.

Searching for a nonzero neutrino mass would then essentially amount to searching for kinks in the photon line profile. This is to some extent similar to looking for kinks in the electron spectra in direct neutrino mass measurement experiments based on CSBD, but instead of measuring electron energies in the keV range, our approach requires measuring photon frequencies corresponding to eV-range energies. An important advantage of our method is that the fractional number of events $\Delta N_{\mathrm{ph}}/N_{\mathrm{ph}}$ in the m_ν-sensitive region scales as $(a_0 - a)/a_0 \simeq m_\nu^2/2Q^2$. That is,

$$\frac{\Delta N_{\mathrm{ph}}}{N_{\mathrm{ph}}} \simeq \frac{m_\nu^2}{2Q^2} \simeq 1.445 \times 10^{-9} (m_\nu/\mathrm{eV})^2 \,. \quad (4.10)$$

For comparison, in tritium CSBD experiments the fractional number of events in the mass-sensitive region scales as $(m_\nu/Q)^3$. Thus, the fractional number of useful events is increased by a very large

factor of order Q/m_ν in our approach compared to the CSBD-based experiments. In particular, for $m_\nu = 1\,\mathrm{eV}$ the fraction of useful photon events is $\sim 10^{-9}$ in the approach proposed here, whereas in BSBD of tritium the fraction of electrons with energies within the last 1 eV below the endpoint energy is $\sim 10^{-13}$.

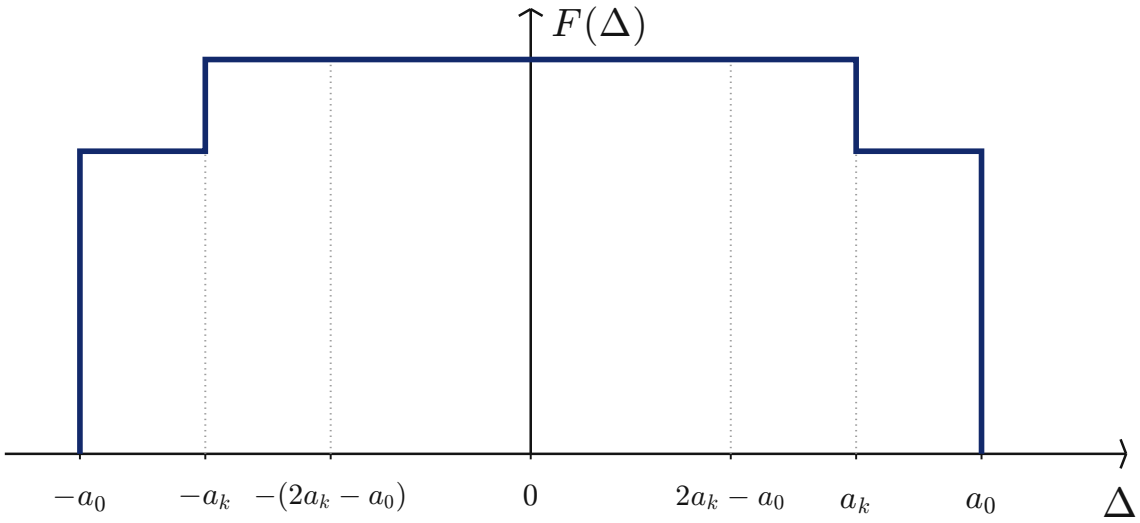

Figure 2: Schematic representation of photon emission line spectrum in the case of one massless and one massive neutrino of mass m_k, in the limit of vanishingly small natural linewidth Γ (not to scale). $\Delta = \omega - \omega_0$; the quantities a_0 and a_k are the velocity parameters a defined in (4.7) for $v = v_0$ and $v = v_k$, respectively. Grey dotted lines mark the borders of the central zone regions of the same widths as those of the wings.

4.3 Statistical requirements in the limit of vanishing natural linewidths

We shall now assess the statistical requirements for measuring neutrino masses within our approach. We do this first in a simplified and idealized manner, assuming that the effects of thermal motion of the parent tritium atoms and the natural linewidths of the relevant atomic states of ^{3}He can be neglected.

Consider a ^{3}He emission line in the case of two neutrino species: one massless neutrino and one massive neutrino of mass m_k (see Fig. 2). We denote by a_0 and a_k the velocity parameters a defined in (4.7) for $v = v_0$ and $v = v_k$, respectively. In the wings of the photon line profile, i.e. in the regions $a_k < |\Delta| < a_0$, only massless neutrinos contribute to the emitted photon spectrum. In the central region, corresponding to $|\Delta| < a_k$, both massless and massive neutrinos contribute, with the weights $1 - |U_{ek}|^2$ and $|U_{ek}|^2$, respectively.

Let N be the full number of the observed photon events corresponding to the atomic transition under discussion. The numbers of events corresponding to the wings and to the central region of the line profile, which we denote by N_w and N_c respectively, are proportional to the integrals of the photon spectrum over these regions, i.e. to the areas of the corresponding parts of the line profile shown in Fig. 2.

To estimate the statistical significance of the neutrino mass determination, we consider the number N_c' of observed photons in the central region of the line profile, but restricted to the intervals in Δ of the same widths as the wings, i.e. in the ranges $2a_k - a_0 < |\Delta| < a_k$. In the limit $m_k = 0$, the spectrum of the studied line is purely rectangular, so the numbers of events in the

spectral intervals of equal widths must coincide. A nonzero difference $N_c' - N_w \simeq N\frac{\Delta v}{v_0}|U_{ek}|^2$ would therefore signify nonvanishing neutrino mass. The statistical significance of observing $m_k \neq 0$ (the number of standard deviations) is then

$$Z = \frac{N_c' - N_w}{\sqrt{N_c' + N_w}} \simeq \frac{\sqrt{N\frac{\Delta v}{v_0}}|U_{ek}|^2}{\sqrt{2 - |U_{ek}|^2}}. \tag{4.11}$$

(see Appendix C for details). The number of observed events required for a significance $k\sigma$ is thus

$$N \simeq k^2 \frac{2 - |U_{ek}|^2}{(\Delta v/v_0)|U_{ek}|^4} = k^2 \frac{4Q^2}{m_k^2|U_{ek}|^4}\big(1 - \frac{1}{2}|U_{ek}|^2\big). \tag{4.12}$$

Consider a sterile neutrino with mass 1 keV and the mixing parameter $|U_{ek}|^2$ equal to $10^{-3}, 10^{-4}$ or 10^{-6}. To achieve a 3σ significance in the observation of a nonzero neutrino mass, the required number of observed photons is then, respectively,

$$N \simeq 1.2 \times 10^{10}\,; \qquad 1.2 \times 10^{12}\,; \qquad 1.2 \times 10^{16}\,. \tag{4.13}$$

As we have ignored here the effects of finite natural linewidth and any possible systematic errors, the numbers in eq. (4.13) should be considered as a minimum requirement.

Let the overall photon detection efficiency for the line under study be $1/\eta$, which means that only a fraction $1/\eta$ of the emitted photons is actually detected. For tritium BSBD transitions to the $1s3s$ state of triplet helium and a tritium source with an activity of 10^{12} Bq (2.8 mg of tritium), the times required to accumulate the numbers of events given in (4.13) are, respectively,

$$0.9\eta \text{ min}\,; \qquad 1.5\eta \text{ hours}\,; \qquad 1.7\eta \text{ yr}. \tag{4.14}$$

If the sterile neutrino mass is 200 eV rather than 1 keV, the required event numbers and the running times of the experiment must be multiplied by a factor of 25.

The above approach can be readily extended to the case of more than two neutrino species. Consider the ordinary active neutrinos with mass eigenvalues m_1, m_2 and m_3. The relevant mixing parameters in this case are

$$|U_{e1}|^2 \simeq 0.7, \qquad |U_{e2}|^2 \simeq 0.3, \qquad |U_{e3}|^2 \simeq 0.022\,. \tag{4.15}$$

In Table 3 the values of the masses of active neutrinos used in our estimates are shown for the normal (NO) and inverted (IO) mass orderings, assuming hierarchical mass spectrum. In this case the masses of the lightest neutrinos are too small to be probed by direct mass measurement experiments. Also, for IO, the masses of the heaviest and next-to-heaviest active neutrinos are too close to each other to be resolved.

	m_1 (eV)	m_2 (eV)	m_3 (eV)
NO	$\simeq 0$	8.7×10^{-3}	0.05
IO	0.0492	0.05	$\simeq 0$

Table 3: Values of masses of active neutrinos used in our sensitivity estimates, assuming hierarchical mass spectrum. NO and IO stand for the normal and inverted mass orderings, respectively.

Using eqs. (4.12), (4.15) together with the neutrino masses given in Table 3, one can determine the numbers of observed events and the corresponding running times of the experiment required to

observe a nonzero neutrino mass at the 3σ significance level. For NO, one obtains

$$N(m_2) \simeq 1.8 \times 10^{15}\,, \qquad t(m_2) \simeq 0.25\eta\,\mathrm{yr} \tag{4.16}$$

$$N(m_3) \simeq 1.0 \times 10^{16}\,, \qquad t(m_3) \simeq 1.4\eta\,\mathrm{yr}\,, \tag{4.17}$$

whereas for IO,

$$N(m_{\nu_1+\nu_2}) \simeq 5.4 \times 10^{13}\,, \qquad t(m_{\nu_1+\nu_2}) \simeq 64\eta\,\mathrm{hours} \tag{4.18}$$

As before, the values of the running time correspond to BSBD transitions to the triplet $1s3s$ excited state of helium atoms and a tritium source with an activity of $10^{12}\,\mathrm{Bq}$.

The simplified consideration presented in this subsection applies to the statistical significance of establishing the existence of kinks in the profile of the studied line, signifying nonzero neutrino masses. The accuracy of measurements of the positions of these kinks, which is essentially the accuracy of determination of the underlying neutrino masses, is determined by the frequency resolution of the lineshape measurements [see eq. (4.9)].

4.4 Effects of finite natural widths of the excited states of ^{3}He

The profiles of the photon lines emitted by ^{3}He atoms take an approximately rectangular shape (in the rest frame of the parent tritium atoms) when the sum Γ of the natural linewidths of the initial and final atomic states of helium is small compared to the maximum Doppler shift $a = (v/c)\omega_0$. However, when analyzing the line profiles to extract the neutrino masses, the condition for neglecting the natural linewidths is much more stringent: Γ must be small not only compared to a, but actually compared to the deviation of a from its value in the limit of massless neutrinos:

$$\Gamma \ll a_0 - a = \frac{\Delta v}{v_0} a_0\,. \tag{4.19}$$

What happens if this condition is not met? As a concrete example, consider the red-line transition $1s3s \to 1s2p$ in triplet helium. For this transition,

$$\omega_0 = 1.755\,\mathrm{eV}\,; \quad \Gamma_i = 1.83 \times 10^{-8}\,\mathrm{eV}\,; \quad \Gamma_f = 6.72 \times 10^{-9}\,\mathrm{eV}\,; \quad \Gamma = \Gamma_i + \Gamma_f = 2.5 \times 10^{-8}\,\mathrm{eV}\,. \tag{4.20}$$

The maximum Doppler shifts for a massless neutrino and for a neutrino with mass $m_k = 1\,\mathrm{keV}$ are

$$a_0 = \frac{v_0}{c}\omega_0 = 1.16 \times 10^{-5}\,\mathrm{eV}; \qquad a_k = a_0(1 - 1.45 \times 10^{-3})\,. \tag{4.21}$$

Thus, although Γ is much smaller than a_0, it is comparable to the difference $a_0 - a_k \simeq 1.7 \times 10^{-8}$ eV. Figure 3 shows the photon spectrum obtained from eqs. (4.6) and (4.7) using the physical natural linewidth $\Gamma = 2.5 \times 10^{-8}\,\mathrm{eV}$ in both panels. The left panel shows the full spectrum over both Doppler edges, whereas the right panel shows the region near the high-frequency edge, $\Delta \in [a_0 - 3\Gamma,\, a_0 + 3\Gamma]$. The red and blue curves correspond to a massless neutrino and a neutrino with mass $1\,\mathrm{keV}$, respectively. One can see that the difference between the massless and massive neutrino cases is still quite noticeable, though distinguishing between them may require rather high event statistics.

The approximations entering the calculation are those stated above: the parent tritium atom is taken to be at rest, Doppler shifts are retained to first order in v/c, recoil directions are isotropically averaged, and thermal broadening, collisional de-excitation, detector resolution, and instrumental frequency calibration errors are not included. These effects must be added separately before the profile can be interpreted as a complete experimental response function.

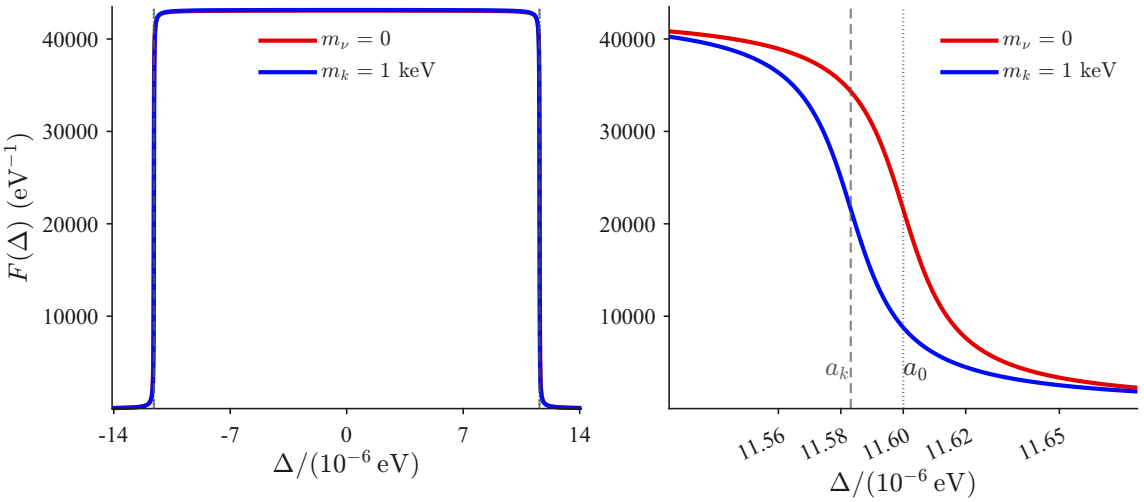

Figure 3: Frequency spectrum of photons from the $1s3s \to 1s2p$ transition in triplet helium. Red and blue curves correspond to a massless neutrino and a neutrino mass eigenstate with $m_k = 1\,\mathrm{keV}$, respectively. Left panel: full spectrum over both Doppler edges, $\Delta \in [-a_0 - 100\Gamma,\, a_0 + 100\Gamma]$; right panel: zoom on the high-frequency endpoint, $\Delta \in [a_0 - 3\Gamma,\, a_0 + 3\Gamma]$. Both panels use $\Gamma = 2.5 \times 10^{-8}\,\mathrm{eV}$. Including theoretical or experimental natural-width uncertainties (0.01% or 3%, respectively) leads to the uncertainty bands that are narrower than, or comparable to, the plotted line thickness on this scale.

4.5 Statistical requirements with finite linewidths

The box-counting estimate introduced in Sec. 4.3 provides a useful starting point because it directly shows how the statistical sensitivity depends on $|U_{ek}|^2$ and m_k^2. However, it applies when the linewidth Γ is smaller than, or comparable to, the mass-induced edge displacement $a_0 - a_k$. For light-neutrino mass measurements, this condition is not necessarily satisfied, and a more refined statistical treatment is therefore required. For a finite natural linewidth, the relevant normalized profile is the function $F(\Delta; a, \Gamma)$ in eq. (4.6). We define the mixed two-component spectrum as

$$F_{\mathrm{mix}}(\Delta) = \left(1 - |U_{ek}|^2\right) F(\Delta; a_0, \Gamma) + |U_{ek}|^2 F(\Delta; a_k, \Gamma)\,, \tag{4.22}$$

and compare it with the zero-neutrino-mass null spectrum

$$F_0(\Delta) = F(\Delta; a_0, \Gamma)\,, \tag{4.23}$$

where $|U_{ek}|^2$ is the electron-flavor admixture of the massive eigenstate. The observable deformation is therefore the ratio

$$\frac{F_{\mathrm{mix}}(\Delta)}{F_0(\Delta)} = \left(1 - |U_{ek}|^2\right) + |U_{ek}|^2\, \frac{F(\Delta; a_k, \Gamma)}{F(\Delta; a_0, \Gamma)}\,. \tag{4.24}$$

This ratio, rather than the absolute profile alone, most directly reveals the spectral distortion induced by nonzero neutrino masses relative to the reference spectrum obtained by setting all neutrino masses to zero.

We use a Fisher-integral estimator to convert a fixed spectral deformation into the number of detected photons required for a target statistical significance. Let $F_0(\Delta)$ be the normalized null spectrum and $F_1(\Delta)$ the normalized alternative spectrum that takes neutrino masses into account, with $\int F_i(\Delta)\, d\Delta = 1$. If N photons are detected in the line, the expected counts in an interval

$d\Delta$ are $NF_i(\Delta)d\Delta$. For Poisson statistics and small bin-by-bin differences, the leading likelihood expansion gives

$$Z_{\rm F}^2 \simeq N\,\mathcal{I}\,, \qquad \mathcal{I} = \int d\Delta\, \frac{[F_1(\Delta) - F_0(\Delta)]^2}{F_0(\Delta)}\,, \tag{4.25}$$

where $Z_{\rm F}$ is the expected Gaussian-equivalent statistical separation for the fixed pair of spectra. The required statistics are then $N_{\rm req}(Z_{\rm F}) = Z_{\rm F}^2/\mathcal{I}$. The integral $\mathcal{I}$ is dimensionless; all finite-linewidth applications of the estimator below include both Doppler edges unless stated otherwise.

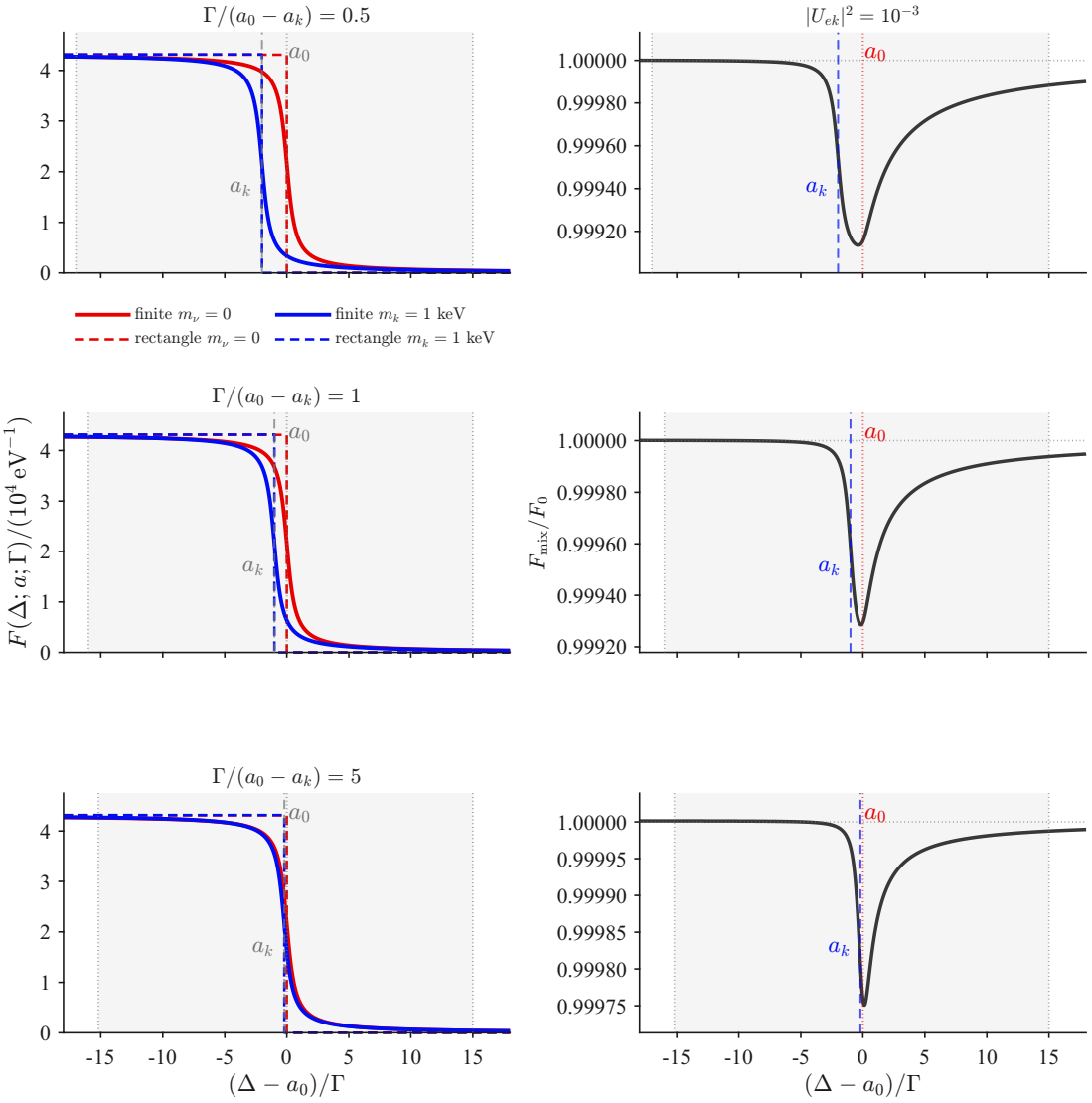

Figure 4: Finite-linewidth spectra entering the Fisher-integral estimator for a benchmark $m_k = 1\,\text{keV}$ neutrino. Rows correspond to $\Gamma/(a_0 - a_k) = 0.5, 1, 5$. The left panels show the finite-linewidth spectra and ideal rectangle limits; the right panels show the observable ratio $F_{\rm mix}/F_0$ for $|U_{ek}|^2 = 10^{-3}$; the shaded region is the one-edge integration interval. The quoted statistics use both Doppler edges by symmetry.

For $m_k = 1\,\text{keV}$, $|U_{ek}|^2 = 10^{-3}$, and $Z_{\rm F} = 3$ (which corresponds to 3σ significance), the box-counting estimate of Sec. 4.3 gives $N_{\rm req} = 1.24 \times 10^{10}$ detected photons. Evaluating Eq. (4.25)

for the corresponding zero-linewidth rectangular spectra over the full profile gives $N_{\rm req} = 6.20 \times 10^9$. Replacing the rectangular spectra by the finite-linewidth profiles $F(\Delta; a, \Gamma)$ of Eq. (4.6) in Eq. (4.22) and including both Doppler edges gives $N_{\rm req} = 9.89 \times 10^9$, 1.35×10^{10}, and 4.54×10^{10} for $\Gamma/(a_0 - a_k) = 0.5$, 1, and 5, respectively. Thus, the box-counting estimate remains close to the Fisher-integral estimator as long as the mass-induced spectral features remain resolved or only weakly broadened, but deviates once Γ becomes significantly larger than $a_0 - a_k$. For the triplet $1s3s \to 1s2p$ transition discussed in the previous subsection, $a_0 - a_k = 1.68 \times 10^{-8}\,\mathrm{eV}$ for $m_k = 1\,\mathrm{keV}$, while $\Gamma = 2.5 \times 10^{-8}\,\mathrm{eV}$. Thus $\Gamma/(a_0 - a_k) = 1.49$, so the edge is moderately smeared but not lost. For $|U_{ek}|^2 = 10^{-3}$ and $Z_{\rm F} = 3$, the box-counting estimate gives $N_{\rm req} = 1.24 \times 10^{10}$ detected photons, whereas the application of the Fisher-integral estimator to both Doppler edges gives $N_{\rm req} = 1.72 \times 10^{10}$. The box approximation provides a reasonable statistical scale for this transition, while the Fisher-integral estimator requires a slightly larger exposure because it accounts for finite-linewidth smearing through Eq. (4.24).

For active-neutrino masses, the edge displacements are much smaller than the triplet $1s3s \to 1s2p$ natural linewidth, so the statistical requirement cannot be assessed from resolved intervals. The relevant observable is instead the finite-linewidth spectral ratio, and the appropriate sensitivity estimator is the Fisher integral of Eq. (4.25). For three active neutrinos, the two-component spectrum in Eq. (4.22) is replaced by an incoherent sum over the three mass eigenstates, with coefficients $|U_{ek}|^2$ fixed by oscillation data. Figure 5 compares the resulting spectrum with the reference spectrum obtained by setting all three neutrino masses to zero. For illustration, we consider inverted ordering with $m_{\rm lightest} = m_3 = 10.0\,\mathrm{meV}$, $\Delta m^2_{21} = 7.41 \times 10^{-5}\,\mathrm{eV}^2$, and $|\Delta m^2_{31}| = 2.44 \times 10^{-3}\,\mathrm{eV}^2$. This gives $(m_1, m_2, m_3) = (50.4, 51.1, 10.0)\,\mathrm{meV}$ and corresponding edge shifts of $(43, 44, 1.7) \times 10^{-18}\,\mathrm{eV}$. Because these shifts are approximately nine orders of magnitude smaller than the natural linewidth of the triplet transition, the ideal box approximation is inadequate and the Fisher-integral estimator must be used. Integrating the Fisher density over finite windows around both Doppler edges yields a statistical requirement of $N^{\Gamma}(3\sigma) = 1.9 \times 10^{21}$ detected photons.

All event counts quoted in this subsection represent purely statistical lower bounds. A complete experimental sensitivity assessment must also account for thermal broadening, detector response, frequency calibration, acceptance, backgrounds, and correlations among nuisance parameters. The statistical requirements therefore appear feasible for keV-scale sterile-neutrino benchmarks when the spectral edges remain resolved or only weakly broadened. By contrast, in the active three-neutrino case for the physical triplet red-line channel, the natural linewidth strongly suppresses the observable spectral deformation; control of systematic uncertainties will therefore be crucial for any realistic sensitivity assessment.

4.6 Effects of thermal motion of parent tritium atoms

The one-to-one correspondence between the neutrino mass and the velocity of the produced ^{3}He atoms holds only in the rest frame of the parent tritium atoms. In the laboratory frame, thermal motion of tritium must be taken into account. We therefore consider how this motion modifies the photon line profile. Let $\vec{v} = v_k \hat{v}$ be the helium recoil velocity in the rest frame of the parent tritium atom, $\vec{v}_T$ the parent velocity in the laboratory, and $\hat{\mathbf{n}}_\gamma$ the detected photon direction. In the laboratory, the helium atom inherits the translational velocity of the parent atom in addition to its BSBD recoil velocity. To first order in the velocities, the Doppler detuning of a photon is proportional to the component of the total helium velocity along the detected photon direction. Since this laboratory velocity is $v_k \hat{v} + \vec{v}_T$, the leading Doppler detuning is

$$\Delta \simeq \frac{\omega_0}{c} \left(v_k \cos\theta + v_{T\parallel} \right), \qquad \cos\theta \equiv \hat{v} \cdot \hat{\mathbf{n}}_\gamma, \qquad v_{T\parallel} \equiv \vec{v}_T \cdot \hat{\mathbf{n}}_\gamma. \tag{4.26}$$

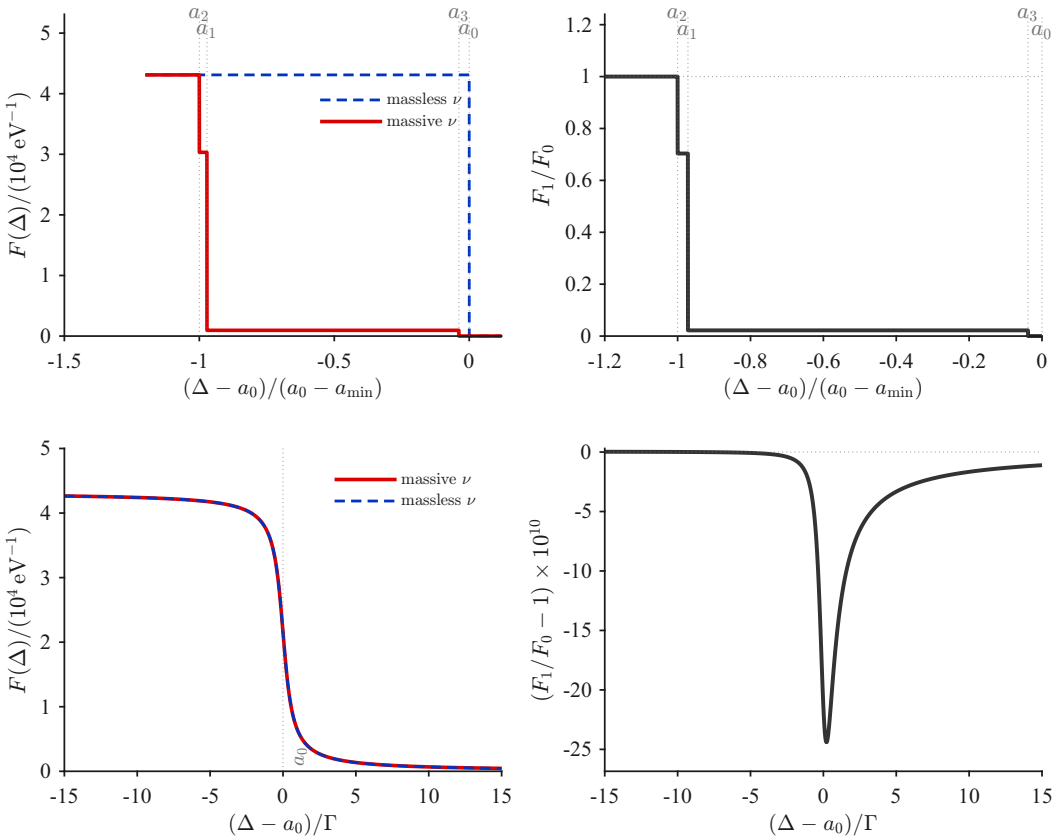

Figure 5: Comparison of the predicted photon spectra for three active neutrinos with inverted mass ordering and $m_3 = 10\,\mathrm{meV}$, relative to the reference case of three massless neutrinos. For the inverted ordering considered here, the lowest kinematic edge is $a_{\min} = a_2$. The upper-left panel shows the ideal rectangular spectra, and the upper-right panel shows their ratio. The lower-left panel shows the corresponding finite-linewidth spectra $F(\Delta)$ for the triplet-helium $1s3s \to 1s2p$ transition, while the lower-right panel shows the relative deviation of their ratio from unity. Using the Fisher-integral estimator, the photon count required for a 3σ statistical discrimination is 1.9×10^{21}.

For an isotropic Maxwell–Boltzmann distribution, $v_{T\parallel}$ is a Gaussian random variable with

$$\langle v_{T\parallel} \rangle = 0, \qquad \langle v_{T\parallel}^2 \rangle = \frac{k_B T}{M_i} = \frac{v_{th\mathrm{T}}^2}{3}. \tag{4.27}$$

Here $v_{th\mathrm{T}} = \sqrt{3k_B T/M_i}$ is the three-dimensional root-mean-square (rms) thermal speed. The leading thermal photon frequency width is therefore

$$\sigma_{\mathrm{th}} = \frac{\omega_0}{c}\sqrt{\frac{k_B T}{M_i}} = \frac{\omega_0}{c}\frac{v_{th\mathrm{T}}}{\sqrt{3}}\,. \tag{4.28}$$

We first neglect the natural linewidth, $\Gamma = 0$, in order to isolate the effect of finite temperature. If $G_T(\epsilon)$ denotes the normalized Gaussian with rms width σ_{th}, the rectangular profile in Eq. (4.8) is replaced by

$$P_{T,k}^{(0)}(\Delta) = \int_{-\infty}^{\infty} d\epsilon\, F_0(\Delta - \epsilon; a_k) G_T(\epsilon) = \frac{1}{4a_k}\left[\mathrm{erf}\left(\frac{\Delta + a_k}{\sqrt{2}\sigma_{\mathrm{th}}}\right) - \mathrm{erf}\left(\frac{\Delta - a_k}{\sqrt{2}\sigma_{\mathrm{th}}}\right)\right]. \tag{4.29}$$

Here $F_0(\Delta; a_k)$ denotes the zero-linewidth rectangular spectrum. Thus, finite temperature smooths both kinematic edges with a width that scales as $\sqrt{T}$, but it does not shift the line center or the kinematic edge reference positions $\Delta = \pm a_k$.

A useful dimensionless measure of the thermal smearing is $\mathcal{R}_T \equiv (a_0 - a_k)/\sigma_{\rm th}$, where $a_0 - a_k$ is the inward displacement of one edge caused by the neutrino mass, while $\sigma_{\rm th}$ is the one-standard-deviation thermal width. Values $\mathcal{R}_T \ll 1$ indicate that the mass-dependent edge displacement is small compared with the thermal smoothing scale.

Figure 6 illustrates this effect for atomic tritium at $T = 1\,\mathrm{K}$, comparing $m_k = 0$ and $m_k = 1\,\mathrm{keV}$. At this temperature, $\sigma_{\rm th} = 0.31\,\mu\mathrm{eV}$, whereas the mass-induced displacement of one edge is only $a_0 - a_k = 0.017\,\mu\mathrm{eV}$, giving $\mathcal{R}_T = 0.055$. Thermal motion therefore strongly smooths the mass-dependent structure, in direct analogy with the degradation caused by a finite natural linewidth discussed in Sec. 4.4. If the temperature is known exactly, the broadened hypotheses remain distinct, and a larger photon sample can in principle reach a chosen statistical significance, although the required event count may become prohibitively large. Uncertainties in the temperature or detector response can introduce additional degeneracies that cannot in general be overcome by statistics alone.

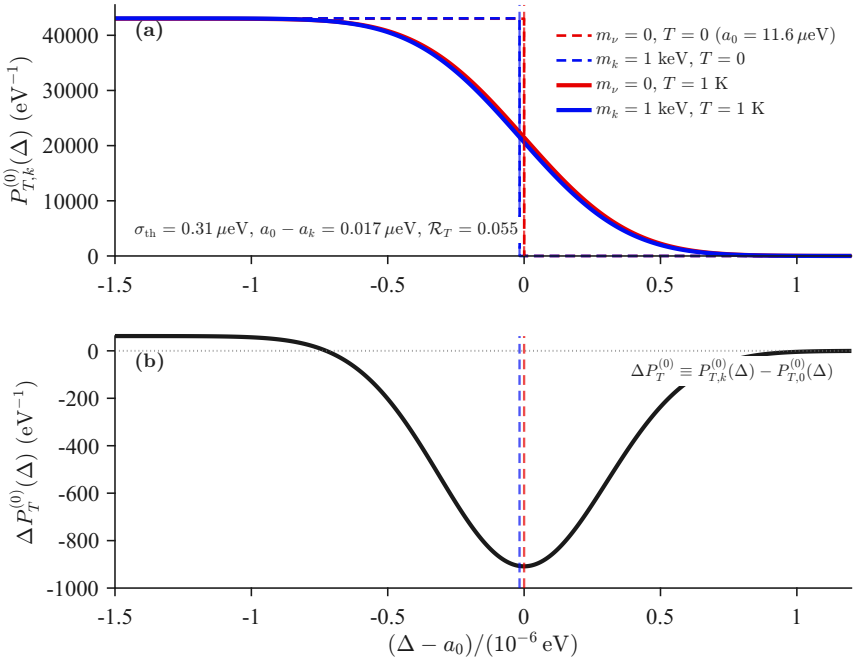

Figure 6: High-frequency edge of the normalized atomic-tritium BSBD photon spectrum for $m_k = 0$ and $m_k = 1\,\mathrm{keV}$. Dashed curves and vertical lines show the ideal $T = 0$, $\Gamma = 0$ rectangular-spectrum edges; solid curves show the leading Gaussian thermal broadening at $T = 1\,\mathrm{K}$, also with $\Gamma = 0$, in order to isolate the temperature effect. The lower panel gives the absolute difference between the two thermally broadened spectra. For this benchmark, $\sigma_{\rm th} = 0.31\,\mu\mathrm{eV}$, $a_0 - a_k = 0.017\,\mu\mathrm{eV}$, and $\mathcal{R}_T \equiv (a_0 - a_k)/\sigma_{\rm th} = 0.055$; thus $\mathcal{R}_T$ is the ratio of the mass-induced displacement of one edge to the thermal rms width.

We now include the natural linewidth. The finite radiative lifetimes of the initial and final helium states give the emitted photon a Lorentzian frequency distribution, whereas the line-of-sight thermal velocity of the parent atom produces the Gaussian Doppler shift described above. These two types of fluctuations have distinct physical origins and are statistically independent in the

present approximation. Their probability distributions must therefore be convolved, so that the finite-temperature profile is

$$P_{T,k}(\Delta) = \int_{-\infty}^{\infty} d\epsilon\, F(\Delta - \epsilon; a_k, \Gamma) G_T(\epsilon)\,. \tag{4.30}$$

The complete profile therefore results from applying both the natural Lorentzian broadening and the thermal Gaussian broadening to the rectangular recoil spectrum. It is not a single Voigt peak, although each kinematic edge is broadened with a Voigt shape. Because both broadening distributions are centered and symmetric, they smooth the kinematic edges without shifting their reference positions $\Delta = \pm a_k$; neither effect therefore produces an intrinsic displacement of the edge location.

For the $m_k = 1\,\mathrm{keV}$ benchmark, a useful temperature scale can be defined by requiring the thermal Gaussian FWHM not to exceed the natural Lorentzian FWHM. For a Gaussian proportional to $\exp[-\epsilon^2/(2\sigma_{\mathrm{th}}^2)]$, the half-maximum occurs at $|\epsilon| = \sqrt{2\ln 2}\,\sigma_{\mathrm{th}}$. Its full width at half maximum is therefore $\Gamma_{\mathrm{G}}^{\mathrm{th}} = 2\sqrt{2\ln 2}\,\sigma_{\mathrm{th}}$. The natural linewidth Γ used in Eq. (4.4) is also a full width at half maximum. A like-for-like comparison therefore requires $\Gamma_{\mathrm{G}}^{\mathrm{th}} \leq \Gamma$. For the red-line transition of Eq. (4.20), with $\omega_0 = 1.755\,\mathrm{eV}$ and $\Gamma = 2.5 \times 10^{-8}\,\mathrm{eV}$, this condition gives

$$T \leq T_{\mathrm{max}} = \frac{M_i}{k_B}\left[\frac{\Gamma}{2\sqrt{2\ln 2}\,\omega_0}\right]^2 = 1.2\,\mathrm{mK}\,. \tag{4.31}$$

This value is independent of the neutrino mass; the choice $m_k = 1\,\mathrm{keV}$ only specifies the kinematic edge illustrated below. The criterion prevents the thermal Gaussian FWHM from exceeding the intrinsic natural width, but it does not make the thermal contribution negligible. As shown in Fig. 7, at $T = T_{\mathrm{max}}$ the combined box–Voigt edge is broader than either the natural-only or thermal-only edge.

To quantify the corresponding statistical degradation in the same idealized framework, we apply the Fisher-integral estimator of Eq. (4.25) to the three-active-neutrino inverted-ordering benchmark considered in Sec. 4.5, now including both the natural linewidth and thermal Doppler broadening at the fixed temperature $T = 1.2\,\mathrm{mK}$. The resulting kinematic edges have a Voigt shape. Integrating the Fisher density over the same finite windows around both Doppler edges gives $N^{\Gamma+T}(3\sigma) = 2.3 \times 10^{21}$ detected photons, compared with $N^{\Gamma}(3\sigma) = 1.9 \times 10^{21}$ for the natural-linewidth-only case. Thus, for this benchmark and an exactly known temperature, thermal broadening increases the purely statistical event requirement by approximately 21%. At 90% C.L. ($Z_{\mathrm{F}} = 1.64$), the corresponding requirement is 6.9×10^{20} detected photons. Using the red-photon production rate of Eq. (2.3) and three years of continuous operation, this requires a constant source inventory of 1.8×10^{25} tritium atoms, equivalent to approximately 88 g of atomic tritium and 2.9×10^5 times the inventory of the KATRIN WGTS source[6].

This linewidth criterion is only a useful scale benchmark, not an experimental sensitivity calculation. The neutrino mass must be inferred by fitting the position and shape of the measured edge. A quantitative sensitivity and event requirement can only be obtained after specifying the detector response and the relevant systematic effects. They depend on the photon event statistics, the natural linewidth, the instrumental frequency resolution, frequency calibration, backgrounds, acceptance, the actual experimental temperature, and the precision with which this temperature is independently known. Such a setup-dependent joint line-shape analysis is beyond the scope of this work.

[6]The current KATRIN WGTS source, containing approximately 6×10^{19} tritium atoms, would provide an $\mathcal{O}(1\,\mathrm{eV})$ sensitivity within this idealized statistical framework.

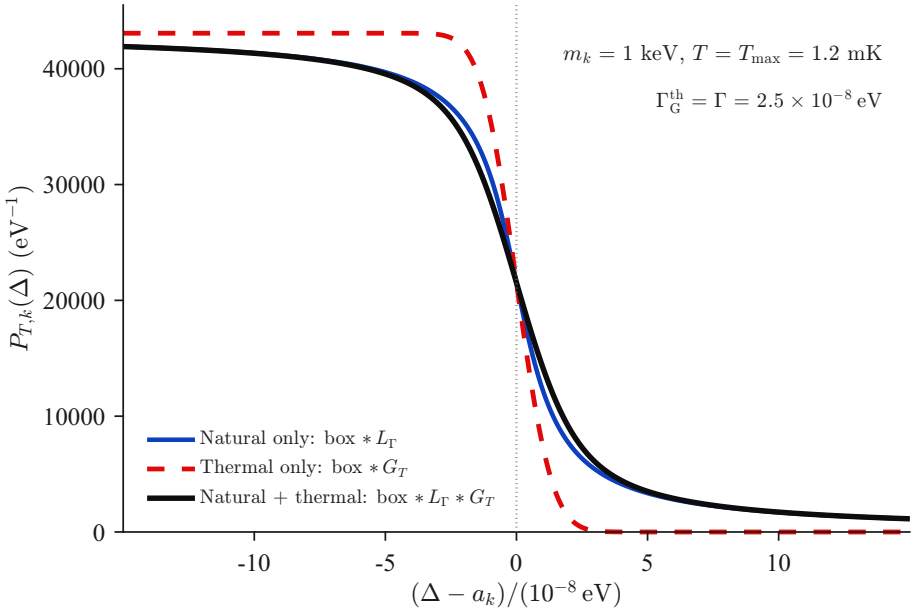

Figure 7: High-frequency edge for $m_k = 1\,\text{keV}$ at $T = T_{\max} = 1.2\,\text{mK}$. The blue curve includes only the natural Lorentzian width, the red dashed curve includes only Gaussian thermal broadening, and the black curve includes both effects through Eq. (4.30). At this temperature, $\Gamma_{\rm G}^{\rm th} = \Gamma = 2.5 \times 10^{-8}\,\text{eV}$. Equality of the two individual FWHM values does not imply that the combined profile has the same width as either component.

5 Summary and discussion

We have proposed a method for the experimental observation of the BSBD of tritium based on the detection of photons emitted by the neutral ^{3}He atoms produced in this process. The key point is that it populates a few low-lying excited states of ^{3}He with significant probabilities. The subsequent radiative decay of these states produces photons that can serve as a clear signature of BSBD.

We have identified the most promising atomic transitions and transition sequences for this purpose: these are the red lines in the spectra of singlet and triplet helium, the NIR line in triplet helium, and their combinations. We have also analyzed possible backgrounds to this detection method and ways to suppress them.

We have proposed a novel method for direct neutrino mass measurement based on the detection of atomic photons emitted by ^{3}He atoms produced in BSBD of tritium. The two-body kinematics of the final state of this process means that, for a given neutrino mass, the emitted neutrino and the helium atom are monoenergetic. The velocity of the helium atom depends weakly on the neutrino mass, so its accurate determination would constitute a neutrino mass measurement.

We propose to measure the velocities of the ^{3}He atoms by observing the Doppler broadening of their photon emission lines. Since electron antineutrinos are linear superpositions of neutrino mass eigenstates with different masses, the spectra of the emitted ^{3}He photons are composite; they must exhibit characteristic kinks corresponding to the onsets of contributions of different neutrino masses. A measurement of the neutrino mass would therefore require an accurate measurement of the photon line profiles. Thus, our approach is based on atomic spectroscopy rather than on measurements of electron energy spectra, as employed by the conventional CSBD-based direct neutrino mass measurement experiments.

As can be seen from eq. (4.9), the currently achieved accuracy in photon line profile measure-

ments, ranging from $\sim 10^{-4}$ to 10^{-11}, implies that neutrino masses in the range from $\sim$18.6 keV down to 30 eV can be probed. Note, however, that the progress in atomic spectroscopy is very rapid, and significant improvements can be expected in the near future.

It should be noted that we used the linear (nonrelativistic) Doppler effect approximation to analyze the sensitivity of our approach to neutrino masses. This approximation remains valid as long as the relativistic corrections to the Doppler shifts are smaller than the distortions of the photon lineshapes induced by a nonzero neutrino mass. This condition holds for $m_\nu \gtrsim (Q^3/M)^{1/2} \simeq 50\,\mathrm{eV}$. To probe smaller neutrino masses, the full relativistic expression for the Doppler frequency shifts must be used. This is completely straightforward and does not lead to any loss of neutrino mass sensitivity of our method.

We have studied the effect of finite natural linewidths on the photon line profiles. Natural broadening smooths the kinematic edges and reduces the spectral difference between neutrino-mass hypotheses, although it does not shift the edge reference positions. For the transitions considered here, this effect makes neutrino-mass measurements below $\mathcal{O}(1\,\mathrm{eV})$ particularly challenging, because the mass-induced edge displacement scales as m_ν^2 and rapidly becomes much smaller than the edge-smearing scale set by the natural linewidth. One possible direction is to identify alternative transitions involving longer-lived atomic states and hence smaller natural linewidths, while accounting for collisional broadening. Another possibility is to revisit laser-induced fluorescence and Doppler absorption spectroscopy, as proposed for tritium BSBD in Ref. [6], and apply Doppler-edge velocimetry [39–41].

Thermal Doppler broadening poses a distinct challenge. The distribution of the parent-atom velocity projected along the detected photon direction produces Gaussian broadening of the kinematic edges, without shifting their reference positions. One possibility – albeit a highly speculative one – would be to employ quantum-sensing technologies and use tagged tritium atoms to accurately measure the velocities of parent atoms prior to their decay. This information could in principle be used to reduce the parent-motion contribution to the Doppler broadening on an event-by-event basis.

Our analysis has focused on describing these physical effects and on identifying the corresponding line-shape scales that can limit a neutrino-mass measurement. The sensitivity of a given experiment is beyond the scope of this work and must be determined from a complete line-shape fit including the setup-specific inputs and systematic effects.

An important advantage of our approach to direct neutrino mass measurement is that the fractional number of events in the neutrino-mass-sensitive region scales as $(m_\nu/Q)^2$. This is to be compared with the fractional number of useful events in the conventional CSBD-based approaches, which scales as $(m_\nu/Q)^3$. Thus, the gain factor is Q/m_ν in our case, which is a very large number, especially for light neutrinos. A disadvantage of our approach is that it imposes more stringent requirements on the acceptable temperature of the tritium source, as discussed above.

In the limit of vanishing neutrino mass, the BSBD photon Doppler edge determines the channel Q-value. For a fixed final atomic state, $\Delta\omega = \omega_0 Q/M$ (where M is the daughter-atom mass and ω_0 the unshifted transition frequency), and thus, $Q = M\Delta\omega/\omega_0$. For independent inputs, the relative uncertainty is $\delta Q/Q = \sqrt{(\delta M/M)^2 + [\delta(\Delta\omega)/\Delta\omega]^2 + (\delta\omega_0/\omega_0)^2}$. For the ^{3}He triplet $1s3s \rightarrow 1s2p$ red transition, $\Delta\omega \simeq 2.8$ GHz. The AME2020 value $\delta M/M = 1.99 \times 10^{-11}$ [42], together with the comparable or smaller fractional uncertainty on ω_0, is negligible relative to the Doppler-edge uncertainty in both benchmarks. Adopting the demonstrated helium red-line precision $\delta(\Delta\omega) = 5$ MHz as an edge-measurement benchmark [43] gives $\delta(\Delta\omega)/\Delta\omega \simeq 1.8 \times 10^{-3}$ and therefore $\delta Q \simeq 33$ eV. Prospectively, helium frequency-comb spectroscopy indicates achievable relative optical-frequency precisions of order 10^{-11} [44], corresponding to absolute uncertainties from a few to a few tens of kilohertz near 706.5 nm. If comparable absolute accuracy can be transferred

to the BSBD Doppler-edge extraction, the channel-Q sensitivity would reach $\mathcal{O}(100\ \mathrm{meV})$, provided that natural-linewidth, thermal, instrumental, calibration, and background effects are controlled at the same frequency scale.

The direct neutrino measurement method proposed in this paper opens a new avenue for determining neutrino masses. Much work still has to be done, however, to establish whether it can constitute a viable alternative to existing methods and achieve sufficiently high sensitivity to neutrino masses.

Acknowledgments

The authors are grateful to Oleg Chkvorets, Jose Crespo López-Urrutia, Guido Drexlin, Jörg Evers, Susanne Mertens, Daniel Murnick, Thomas Pfeifer, Hamish Robertson, Vera Schäfer, Alexei Smirnov and Sergey Vasiliev for very useful and stimulating discussions.

A 2-body decay and the speed of ^{3}He

We use the following notation: $M_i \equiv M(\mathrm{T})$ and $M_f \equiv M(^3\mathrm{He})$ are the atomic masses of tritium and ^{3}He, m_k is mass of the kth neutrino mass eigenstate; $Q \equiv M_i - M_f$. For transitions to an excited atomic state of ^{3}He with the excitation energy E_{exc}, the quantity M_f must be replaced by $M(^3\mathrm{He}) + E_{\mathrm{exc}}$, and the Q-value of the process must be modified accordingly. In the rest frame of the parent tritium the velocity of the ^{3}He atom produced along with neutrino mass eigenstate ν_k is given by

$$v_k = \frac{\left[(M_i^2 - M_f^2)^2 - 2(M_i^2 + M_f^2)m_k^2 + m_k^4\right]^{1/2}}{M_i^2 + M_f^2 - m_k^2}\,. \tag{A.1}$$

Neglecting terms of the fourth and higher order in neutrino mass and taking into account that $Q^2/(M_i^2 + M_f^2) \ll 1$, we arrive at eq. (4.2), which is valid to an accuracy of about 10^{-11}. If higher accuracy is needed, the exact formula (A.1) should be used.

B BSBD with a mixed atomic/molecular tritium source and background from CSBD

We follow the notation of the main text: Γ_1 is the ordinary CSBD decay rate per tritium nucleus, and Γ_2 denotes here the effective BSBD production rate, which includes both singlet and triplet final-state configurations of ^{3}He in the unresolved $1s3s$ states that yield red photons. The numerical benchmark uses $\Gamma_2 = (4/3)\Gamma_2^{\mathrm{triplet}}$. The controlled variable is the atomic fraction k, defined as the fraction of tritium nuclei in atomic form. For a β-activity A,

$$N_0 = \frac{A}{\Gamma_1}, \qquad N_a = kN_0, \qquad N_m = \frac{1}{2}(1-k)N_0, \tag{B.1}$$

where N_0 is the total number of tritium nuclei, N_a the number of atomic tritium atoms, and N_m the number of T_2 molecules. The observable is the red-line photoelectron yield from $^3\mathrm{He}^*(1s3s)$ singlet- and triplet state de-excitations.

The de-excitation of the $1s3s$ state may proceed through radiative or non-radiative channels. Non-radiative losses, photon transport, detector acceptance, optical transmission, collection efficiency, and photosensor quantum efficiency are absorbed into the overall efficiency factor $\varepsilon_{\mathrm{tot}}$. CSBD of T_2 can also populate the same unresolved states, directly or through dissociation, charge rearrangement, secondary excitation, or cascades. This contribution is described by an effective

Quantity	Symbol	Value	Quantity	Symbol	Value
Activity	A	10^9 s^{-1}	CSBD rate	Γ_1	1.786×10^{-9} s^{-1}
Eff. BSBD rate	Γ_2	5.53×10^{-13} s^{-1}	CSBD yield	r	10^{-3}
Atomic scan	k_i	$0, 0.25, 0.50, 0.75$	Exposure/point	t_i	900 s
Efficiency	$\varepsilon_{\rm tot}$	2.4×10^{-3}	Atomic-fraction error	σ_k	0.05

Table 4: Illustrative benchmark used to display the method. The CSBD yield r, scan range, exposure, and uncertainties are given for illustration purposes and should not be interpreted as an experimental forecast.

$1s3s$-production yield r per molecular CSBD decay. A possible modification of the BSBD $1s3s$-production rate in molecular tritium is parameterized as $\Gamma_2^{\rm mol} = (1-\delta)\Gamma_2$.

For an exposure t_i at fixed k_i, the detected photoelectron yield is the photoelectron version of eq. (3.5); the corresponding photon-yield equations, including the $\delta = 0$ limit, have already been given in eqs. (3.5) and (3.6) and are not repeated:

$$N_{\rm pe}(k_i) = N_{\rm ph}(k_i)\,\varepsilon_{\rm tot} = A t_i \varepsilon_{\rm tot}\left[\frac{\Gamma_2}{\Gamma_1} + (1-k_i)\left(r - \frac{\Gamma_2}{\Gamma_1}\delta\right)\right]. \tag{B.2}$$

The detected photoelectron yield, $N_{\rm pe}$, is a linear function of $(1-k)$, with its slope depending in general on the value of δ. For $\delta = 0$ the slope simplifies to $A\,t_i\,\varepsilon_{\rm tot}\,r$. Therefore, in this limit, a scan of the atomic fraction k provides two independent observables through the linear dependence of $N_{\rm pe}$ on $(1-k)$, allowing the extraction of both the effective BSBD production rate Γ_2 and the molecular CSBD yield r. This separation is model-dependent: it assumes that atomic and molecular BSBD have the same effective $1s3s$-production rate per tritium nucleus. If $\delta \neq 0$, the coefficient of $(1-k)$ instead measures $r_{\rm eff} = r - (\Gamma_2/\Gamma_1)\delta$. As discussed in the main text, there are theoretical and phenomenological arguments suggesting that the correction term $\Gamma_2/\Gamma_1\delta$ is expected to be negligible, such that $r_{\rm eff} \approx r$ in practice.

The benchmark value $\varepsilon_{\rm tot} = 2.4\times10^{-3}$ should therefore be interpreted as an effective detection efficiency that a $1s3s$ excitation ultimately produces a detected photoelectron. It is used only to illustrate the analysis framework and should not be interpreted as the performance of a specific detector design.

The statistical treatment can be written in the standard pull-term form

$$\chi^2(\xi,\phi,\eta_A,\eta_\varepsilon,\eta_{k,i}) = \sum_i \frac{\left[N_i - \mu_i(\xi,\phi,\eta_A,\eta_\varepsilon,\eta_{k,i})\right]^2}{\sigma_{{\rm stat},i}^2} + \eta_A^2 + \eta_\varepsilon^2 + \sum_i \eta_{k,i}^2, \tag{B.3}$$

with

$$\mu_i = (1+\eta_A\sigma_A)(1+\eta_\varepsilon\sigma_\varepsilon)\left[\xi + \phi\,(1-k_i-\eta_{k,i}\sigma_k)\right]. \tag{B.4}$$

The fit parameters ξ and ϕ are the nuisance-free intercept and molecular-fraction slope of the linearized yield model, both measured in detected photoelectrons. For the equal-exposure benchmark $t_i = t$, comparison with eq. (B.2) gives

$$\xi = A t \varepsilon_{\rm tot}\frac{\Gamma_2}{\Gamma_1}, \qquad \phi = A t \varepsilon_{\rm tot}\left(r - \frac{\Gamma_2}{\Gamma_1}\delta\right).$$

For unequal exposures, the same parametrization should be applied to exposure-normalized yields or generalized to point-dependent ξ_i and ϕ_i. Here N_i is the detected photoelectron yield at scan point i, and $\sigma_{{\rm stat},i} \simeq \sqrt{N_i}$ for large counts. The nuisance parameters η_A, η_ε, and $\eta_{k,i}$ have unit Gaussian

priors. The benchmark uses fractional normalization widths $\sigma_A = \sigma_\varepsilon = 0.05$ and an absolute point-to-point composition width $\sigma_k = 0.05$. A realistic analysis may instead split the composition uncertainty into correlated calibration and uncorrelated components. For the reference case, the mean generated yields per measurement point are $\langle N_{ph} \rangle = 8.41 \times 10^8$ and $\langle N_{\rm pe} \rangle = 2.02 \times 10^6$. The statistical uncertainty is only $\simeq 0.07\%$, while the combined systematic uncertainty is $\simeq 9.3\%$ for the assumed inputs. This illustrates the generic importance of source-composition and normalization systematics, but does not provide a quantitative sensitivity projection.

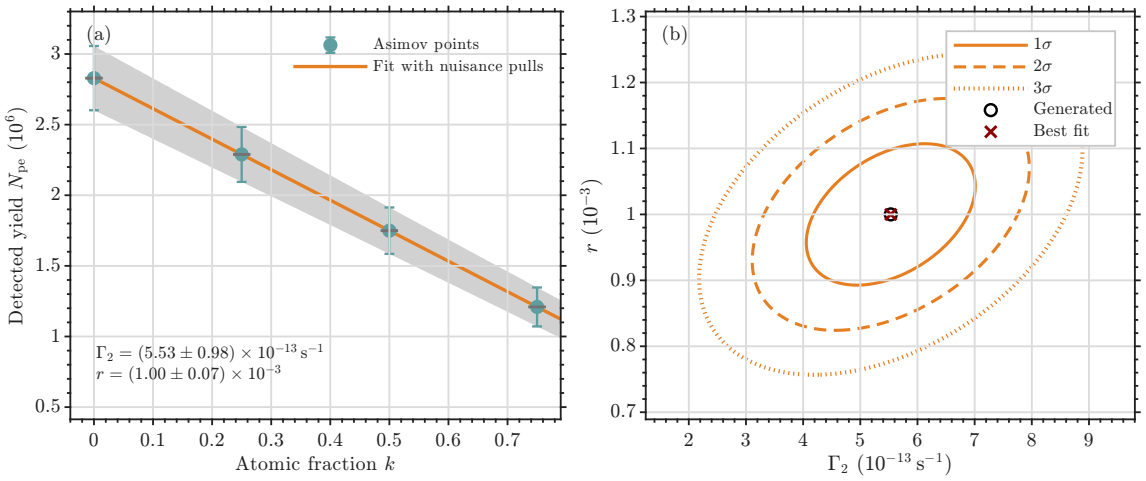

Figure 8: Illustrative atomic-fraction scan for the benchmark configuration. Panel (a): detected photoelectron yield as a function of k, fitted with Eq. (B.2) for $\delta = 0$. The grey band shows the profiled nuisance-pull uncertainty. Panel (b): confidence regions in the (Γ_2, r) plane obtained from $\Delta\chi^2 = \chi^2 - \chi^2_{\rm min}$. The contours are derived from the expected (unfluctuated) photoelectron yields for the benchmark values $\Gamma_2 = 5.53 \times 10^{-13}$ s^{-1} and $r = 10^{-3}$.

For the benchmark configuration considered here, fitting the expected (unfluctuated) yields gives $\Gamma_2 = (5.53 \pm 0.98) \times 10^{-13}$ s^{-1} and $r = (1.00 \pm 0.071) \times 10^{-3}$. The quoted uncertainties are specific to the benchmark configuration considered here, including the assumed value of r, the choice of the four k measurement points, and the adopted nuisance-parameter model. They are therefore intended to illustrate the fitting methodology rather than to represent a projected experimental sensitivity. The method is particularly useful because it separates the two production mechanisms. The linear term in $(1 - k)$ probes the molecular CSBD-induced production of $^3{\rm He}^*(1s3s)$, while the constant term corresponds to the BSBD contribution in the reference model ($\delta = 0$). A quantitative reach requires external experimental inputs, in particular the achievable range and stability of k, the optical collection efficiency, possible non-radiative quenching, the value of r, and non-BSBD optical backgrounds from walls, plasma processes, RF excitation, and delayed fluorescence.

Beyond the BSBD search itself, such a scan could provide an *in-situ* handle on the atomic and molecular fractions in a gaseous tritium source. If calibrated against independent composition measurements, the k-dependent optical response could therefore become a useful source-diagnostics tool for future tritium-based neutrino-mass experimental programs.

C Statistical requirements for neutrino mass measurements

Consider a ^{3}He emission line in the case of two neutrino species: one massless neutrino and one massive neutrino of mass m_k (see Fig. 2). In the wings of the photon line profile ($a_k < |\Delta| < a_0$), contributions from the massive neutrino are kinematically forbidden, and the spectrum of the emitted photons is entirely due to the massless neutrino. In the central region ($|\Delta| < a_k$), both massless and massive neutrinos contribute, with the weights $1 - |U_{ek}|^2$ and $|U_{ek}|^2$, respectively. The heights of the lineshape plateaus in the wings and in the central region, denoted respectively by F_w and F_c, are

$$F_w = \frac{1}{2a_0}\left(1 - |U_{ek}|^2\right) , \qquad F_c = \frac{1}{2a_0}\Big[1 + |U_{ek}|^2 \frac{a_0 - a_k}{a_k}\Big] \;\simeq\; \frac{1}{2a_0}\Big[1 + |U_{ek}|^2 \frac{\Delta v}{v_0}\Big], \quad \text{(C.1)}$$

The height of the steps at $\Delta = \pm a_k$ is therefore

$$\Delta F = F_c - F_w = \frac{1}{2a_0}|U_{ek}|^2\Big(1 + \frac{\Delta v}{v_0}\Big). \quad \text{(C.2)}$$

Let N be the full number of the observed photon events corresponding to the atomic transition under discussion. The numbers of events corresponding to the wings and to the central region of the line profile, which we denote by N_w and N_c, are proportional to the integrals of the photon spectrum over these regions, i.e. to the areas of the corresponding parts of the line profile shown in Fig. 2. From eq. (C.1) we find

$$N_w = N\frac{\Delta v}{v_0}\left(1 - |U_{ek}|^2\right) , \quad N_c = N\Big[1 - \frac{\Delta v}{v_0}\left(1 - |U_{ek}|^2\right)\Big]. \quad \text{(C.3)}$$

To estimate the statistical significance of the neutrino mass determination, consider the number N_c' of observed photons in the central region of the line profile, but restricted to the intervals in Δ of the same widths as the wings, i.e. in the ranges $2a_k - a_0 < |\Delta| < a_k$:

$$N_c' \;=\; \frac{\Delta v/v_0}{1 - \Delta v/v_0} N_c \;\simeq\; N\frac{\Delta v}{v_0}\Big[1 + \frac{\Delta v}{v_0}|U_{ek}|^2\Big]. \quad \text{(C.4)}$$

A nonzero difference $N_c' - N_w \;\simeq\; N\frac{\Delta v}{v_0}|U_{ek}|^2$ would signify nonvanishing neutrino mass. The statistical significance of observing $m_k \neq 0$ (the number of standard deviations) is then

$$Z \;=\; \frac{N_c' - N_w}{\sqrt{N_c' + N_w}} \;\simeq\; \frac{\sqrt{N\frac{\Delta v}{v_0}}|U_{ek}|^2}{\sqrt{2 - |U_{ek}|^2}}. \quad \text{(C.5)}$$

This yields eq. (4.12) for the number of observed events required for significance $k\sigma$.

References

[1] R. Daudel, M. Jean and M. Lecoin, *Sur la possibilité d'existence d'un type particulier de radioactivité phénomène de création e*, *Journal de Physique et le Radium* **8** (1947) 238.

[2] P. Sherk, *Bound electron creation in the decay of tritium*, *Phys. Rev.* **75** (1949) 789.

[3] J.N. Bahcall, *Theory of bound-state beta decay*, *Phys. Rev.* **124** (1961) 495.

[4] K. Takahashi and K. Yokoi, *Nuclear β-decays of highly ionized heavy atoms in stellar interiors*, *Nucl. Phys. A* **404** (1983) 578.

[5] B. Budick, *Atomic effects on the tritium ft value*, *Phys. Rev. Lett.* **51** (1983) 1034.

[6] S. Cohen, D. Murnick and R. Raghavan, *Bound-state beta-decay and kinematic search for neutrino mass*, *Hyperfine Interactions* **33** (1987) 1.

[7] M. Harston and N. Pyper, *Atomic effects on the ft value for tritium β decay*, *Phys. Rev. A* **48** (1993) 268.

[8] K.A. Kouzakov and A.I. Studenikin, *Bound-state beta-decay of neutron in strong magnetic field*, *Phys. Rev. C* **72** (2005) 015502 [hep-ph/0412134].

[9] E.K. Akhmedov, J. Kopp and M. Lindner, *Oscillations of Mössbauer neutrinos*, *JHEP* **05** (2008) 005 [0802.2513].

[10] M. Faber, A.N. Ivanov, V.A. Ivanova, J. Marton, M. Pitschmann, A.P. Serebrov et al., *On continuum-state and bound-state β^- decay rates of the neutron*, *Phys. Rev. C* **80** (2009) 035503 [0906.0959].

[11] J. McAndrew, S. Paul, R. Engels, P. Fierlinger, E. Gutsmiedl, J. Schön et al., *Bound beta-decay of the free neutron: BoB*, *Phys. Procedia* **51** (2014) 37.

[12] A. Gupta, C. Lahiri and S. Sarkar, *Bound and continuum state β^- decay of bare atoms: enhancement of decay rate and changes in β^- decay branching*, *Phys. Rev. C* **100** (2019) 064313 [1808.09717].

[13] S. Liu, C. Gao and C. Xu, *Investigation of bound state β^- decay half-lives of bare atoms*, *Phys. Rev. C* **104** (2021) 024304.

[14] Y. Xiao and L.-J. Wang, *Calculations of bound-state β^--decay half-lives of highly ionized $^{163}Dy^{66+}$, $^{187}Re^{75+}$ and $^{205}Tl^{81+}$*, *Phys. Rev. C* **110** (2024) 054308 [2404.15897].

[15] M. Jung et al., *First observation of bound state beta-decay*, *Phys. Rev. Lett.* **69** (1992) 2164.

[16] F. Bosch et al., *Observation of bound-state beta-decay of fully ionized ^{187}Re: ^{187}Re –^{187}Os cosmochronometry*, *Phys. Rev. Lett.* **77** (1996) 5190.

[17] T. Ohtsubo et al., *Simultaneous measurement of β^- decay to bound and continuum electron states*, *Phys. Rev. Lett.* **95** (2005) 052501.

[18] R.S. Sidhu et al., *Bound-state beta decay of $^{205}Tl^{81+}$ ions and the LOREX Project*, *Phys. Rev. Lett.* **133** (2024) 232701 [2501.06029].

[19] A. Kawasaki, *Quantum sensing using atomic clocks for nuclear and particle physics*, *Appl. Phys. Rev.* **12** (2025) 041331 [2411.19424].

[20] M.C. Marshall et al., *High-stability single-ion clock with 5.5×10^{-19} systematic uncertainty*, *Phys. Rev. Lett.* **135** (2025) 033201 [2504.13071].

[21] H. Bekker, A. Borschevsky, Z. Harman, C.H. Keitel, T. Pfeifer, P.O. Schmidt et al., *Detection of the 5p – 4f orbital crossing and its optical clock transition in Pr^{9+}*, *Nature Commun.* **10** (2019) 5651 [1910.09010].

[22] C. Fredrick, F. Olsen, R. Terrien, S. Mahadevan, F. Quinlan and S.A. Diddams, *Thermal-light heterodyne spectroscopy with frequency comb calibration*, *Optica* **9** (2022) 221.

[23] Thorlabs, "*Fabry - Perot Interferometer Tutorial*." https://www.thorlabs.com/fabry-perot-interferometer-tutorial?tabName=Fabry-Perot%20Tutorial, 2026.

[24] J.A. Formaggio, A.L.C. de Gouvêa and R.G.H. Robertson, *Direct measurements of neutrino mass*, *Phys. Rept.* **914** (2021) 1 [2102.00594].

[25] KATRIN collaboration, *Direct neutrino-mass measurement based on 259 days of KATRIN data*, *Science* **388** (2025) 180 [2406.13516].

[26] PTOLEMY collaboration, *Neutrino physics with the PTOLEMY project: active neutrino properties and the light sterile case*, *JCAP* **07** (2019) 047 [1902.05508].

[27] PROJECT 8 collaboration, *Determining the neutrino mass with cyclotron radiation emission spectroscopy—Project 8*, *J. Phys. G* **44** (2017) 054004 [1703.02037].

[28] A.A.S. Amad et al., *Determining absolute neutrino mass using quantum technologies*, *New J. Phys.* **27** (2025) 105006 [2412.06338].

[29] L. Gastaldo et al., *The Electron Capture* ^{163}*Ho experiment ECHo: an overview*, *J. Low Temp. Phys.* **176** (2014) 876 [1309.5214].

[30] B. Alpert et al., *HOLMES - The electron capture decay of* ^{163}*Ho to measure the electron neutrino mass with sub-eV sensitivity*, *Eur. Phys. J. C* **75** (2015) 112 [1412.5060].

[31] C.J. Martoff et al., *HUNTER: precision massive-neutrino search based on a laser cooled atomic source*, *Quantum Sci. Technol.* **6** (2021) 024008.

[32] A. Kramida, Y. Ralchenko, J. Reader and N.A. Team, "NIST atomic spectra database (ver. 5.12)." [Online]. Available: https://physics.nist.gov/asd, 2024. 10.18434/T4W30F.

[33] S. Jonsell, A. Saenz and P. Froelich, *Neutrino-mass determination from tritium beta decay: Corrections to and prospects of experimental verification of the final-state spectrum*, *Phys. Rev. C* **60** (1999) 034601.

[34] A. Saenz, S. Jonsell and P. Froelich, *Improved molecular final-state distribution of* HeT^+ *for the* β*-decay Process of* T_2, *Phys. Rev. Lett.* **84** (2000) 242.

[35] L.I. Bodine, D.S. Parno and R.G.H. Robertson, *Assessment of molecular effects on neutrino mass measurements from tritium* β *decay*, *Phys. Rev. C* **91** (2015) 035505 [1502.03497].

[36] TRIMS collaboration, *Beta decay of molecular tritium*, *Phys. Rev. Lett.* **124** (2020) 222502 [2001.11671].

[37] I.A. Kotelnikov and A.I. Milstein, *Electron radiative recombination with a hydrogen-like ion*, *Physica Scripta* **94** (2019) 055403 [1810.08071].

[38] F. Gluck, *Order-*α *radiative correction calculations for unoriented allowed nuclear, neutron and pion beta decays*, *Comput. Phys. Commun.* **101** (1997) 223.

[39] B.M. Gentry and C.L. Korb, *Edge technique for high-accuracy Doppler velocimetry*, *Applied Optics* **33** (1994) 5770.

[40] J.A. McKay, *Modeling of direct detection Doppler wind lidar. I. The edge technique*, *Applied Optics* **37** (1998) 6480.

[41] M.J. McGill and J.D. Spinhirne, *Comparison of two direct-detection Doppler lidar techniques*, *Optical Engineering* **37** (1998) 2675.

[42] M. Wang, W.J. Huang, F.G. Kondev, G. Audi and S. Naimi, *The AME 2020 atomic mass evaluation (II). Tables, graphs and references*, *Chin. Phys. C* **45** (2021) 030003.

[43] K. Thomas, J. Ross, B. Henson, D. Shin, K.G.H. Baldwin, S.S. Hodgman et al., *Direct*

measurement of the forbidden $2^3S_1 \to 3^3S_1$ *atomic transition in helium*, *Phys. Rev. Lett.* **125** (2020) 013002 [2002.04811].

[44] P. Cancio Pastor, L. Consolino, G. Giusfredi, P. De Natale, M. Inguscio, V.A. Yerokhin et al., *Frequency metrology of helium around 1083 nm and determination of the nuclear charge radius*, *Phys. Rev. Lett.* **108** (2012) 143001 [1201.1362].